

Thesis for the Degree of Master of Science

**Development of the Infrared Wide-Field
Off-Axis Reflecting Telescope**

Sanghyuk Kim

Department of Astronomy and Space Science

Graduate School

Kyung Hee University

Suwon, Korea

February, 2009

Development of the Infrared Wide-Field Off-Axis Reflecting Telescope

Sanghyuk Kim

Department of Astronomy and Space Science

Graduate School

Kyung Hee University

Suwon, Korea

February, 2009

Development of the Infrared Wide-Field Off-Axis Reflecting Telescope

by

Sanghyuk Kim

Advised by

Dr. Soojong Pak

Submitted to the Department of Astronomy and Space Science
and the Faculty of the Graduate School of Kyung Hee University
in partial fulfillment of the requirements for degree of
Master of Science

Dissertation Committee

Dr. Soojong Pak

Dr. Minhwan Jang

Dr. Goen Hee Kim

Acknowledgment

이 논문을 완성하기까지 정말 많은 분들의 도움이 있었습니다. 2 년간의 석사과정을 마치며 제가 무사히 논문 완성할 수 있게 도움을 주신 많은 분들께 감사 드립니다.

가장 먼저 부족한 저에게 칭찬과 격려를 아끼지 않으시며 석사과정에 입학하기 전부터 지금까지 저를 지도해주시고 이끌어주신 박수종 교수님께 진심 어린 감사와 존경의 마음을 전하고 싶습니다. 힘들고 어려웠던 시기도 있었지만 교수님의 충고와 따뜻한 관심이 있었기에 이렇게 논문을 마치며 감사의 글을 쓸 수 있게 되었습니다. 또한 교수님께서 보여주신 자기관리 방법과 제가 앞으로 공부를 계속하기 위해 알고 지켜야 할 것들에 대한 말씀 잊지 않고 계속 지켜나가겠습니다. 그리고 학부시절부터 지금까지 참된 학자와 교육자로서의 모범을 보여주신 김갑성 교수님, 김상준 교수님, 김성수 교수님, 김원규 교수님, 문용재 교수님, 민영기 교수님, 이동훈 교수님, 장민환 교수님, 최광선 교수님께 감사 드립니다.

석사과정 동안 제 논문과 연구가 결실을 맺을 수 있도록 도와주신 한국기초과학지원 연구원 초정밀가공팀의 김건희 부장님, 김효식 형님 장기수 박사님, 양성환 형, 김민자누나, 이상용 형, 김명상 형, 국명호 형, 정준오 형 그리고 복민갑 형, 이인제 형, 이선규, 길준덕에게 너무나도 감사 드립니다. 팀원 분들께서 보여주신 따뜻한 관심과 배려 그리고 도움에 보답하기 위해 앞으로 성실하고 열심히 하는 모습 보여드리겠습니다.

적외선 실험실에서 좋은 동료들과 연구를 할 수 있었다는 것은 저에게 큰 행복이었습니다. 연구실이 처음 생겼을 때부터 지금까지 함께한 권정미 누나와 고현주, 항상 저를 도와주고 챙겨주신 이용석 형과 김은빈 누나, 친한 동기이자 연구실 동료인 김재영, 오희영 그리고 지금은 학교에 계시지 않지만

석사과정에 처음 입학했을 때 많은 도움과 조언을 주신 김대욱 형에게 감사의 마음을 전합니다. 또한, 제가 궁금한 것이 있을 때마다 친절하게 도와주신 공간물리연구실의 이재형 선배, 천체물리연구실의 이지원 선배, 신지혜 선배, 우주기상연구실의 이경선 선배를 비롯한 우주과학과의 모든 연구실 선후배 및 동기 분들에게 감사 드립니다.

경희대학교 우주과학과에 입학해서 지금까지 03 학번 동기들을 비롯한 선후배 분들 그리고 친구들과 함께 했던 시간들이 있었기에 대학생살이 저에게 즐거운 추억으로 남을 수 있을 것 같습니다. 그리고 제가 힘들 때 조언과 격려를 아끼지 않고 제가 기쁠 때 함께 기뻐해준 김상민, 김은비, 김재현 형, 김준오, 김태현, 문기석 형, 민현우 형, 서영후, 이병훈, 이준우 형, 이준현, 전제현, 전채우, 조영학 형에게 다시 한번 감사의 마음을 전하고 싶습니다. 국민학교 시절부터 지금까지 함께 했던 권민호, 송진얼, 정상엽, 홍성연을 비롯한 이때 뛰어 친구들에게 큰 고마움을 전합니다. 그리고 종로학원에서 1 년간 함께 공부했던 유경모, 이석원, 좌태욱, 최재원에게도 고맙다는 말을 전합니다. 대학원에 입학하기 전 미국에서 많은 조언을 주신 조일성 박사님께 감사 드리며 한달 간 함께 일했던 서정은, 윤영혁 형, 임선인, 정애라, 최은정 그리고 운노상과의 추억과 대형 과제에 조금이나마 참여했던 경험은 제게 큰 도움이 되었습니다. 그리고 석사과정에 채 입학하기도 전에 좋은 경험을 쌓게 해주신 박수종 교수님께 다시 한번 감사 드립니다.

마지막으로 지금의 제가 있을 수 있게 낳아주시고 무한한 사랑과 애정으로 키워주신 어머니, 아버지 진심으로 감사 드리고 사랑합니다.

2008 년 겨울
김상혁 드림

Abstract

We have developed the infrared wide-field off-axis reflecting telescope based on the Schwarzschild-Chang type. Off-axis reflecting telescopes have advantages in infrared comparing with refracting or on-axis reflecting telescopes. The off-axis mirrors of our telescope are fabricated at Korea Basic Science Institute (KBSI). This is the first attempt to directly manufacture as off-axis asymmetric segments in Korea. We analyzed for the measured data of the fabricated mirror surfaces using the MPFIT_2D procedure in IDL, and fitted the polynomial surface functions to the surface data points of the fabricated mirrors. We applied the derived surface functions to the surface parameters of the Schwarzschild-Chang type design in the ray-tracing program. We have accomplished alignment of the two-mirror off-axis reflecting telescope using a ray tracing method. Finally, we performed point source test and compare the point source image with the result of the simulation.

Contents

Acknowledgment	i
Abstract	iii
Chapter 1 Introduction	1
Chapter 2 Design and tolerance analysis	4
2.1 The Schwarzschild-Chang reflecting telescope	4
2.2 Tolerance analysis	9
Chapter 3 Fabrication of off-axis mirror	13
3.1 The backside structure of the off-axis reflecting mirrors.....	13
3.2 Machining off-axis reflecting mirrors.....	16
3.3 Measurement of off-axis reflecting mirrors	18
3.4 Numerical format of the measured mirror surfaces	22
Chapter 4 Summary and Conclusion	31
4.1 Manufacturing of the alignment system	31
4.2 Optimization and tolerance analysis using fitted mirrors.....	35
4.3 The ray tracing method for alignment	37
Chapter 5 Point source test and result	44
Conclusion	49
Bibliography	51

List of Figures

Figure 2.1 Layout of the Schwarzschild-Chang type off-axis reflecting telescope .	6
Figure 2.2 Spot diagram of the Schwarzschild-Chang type off-axis reflecting telescope for various fields.....	7
Figure 2.3 MTF of the Schwarzschild-Chang type off-axis reflecting telescope for various fields	8
Figure 2.4 Tolerances of the Schwarzschild-Chang type off-axis reflecting telescope.....	11
Figure 3.1 Secondary mirror stage	14
Figure 3.2 Backside structure of the secondary mirror	15
Figure 3.3 Machining image of the primary mirror	17
Figure 3.4 Primary mirror of the off-axis reflecting telescope	19
Figure 3.5 Secondary mirror of the off-axis reflecting telescope	20
Figure 3.6 Intensity map of the designed primary mirror surface function.....	23
Figure 3.7 Intensity map of the designed secondary mirror surface function	24
Figure 3.8 Intensity map of the fitted primary mirror surface function	25
Figure 3.9 Intensity map of the derived secondary mirror surface function.....	26
Figure 3.10 Sag difference of the designed and fitted primary mirror surface function.	
(a) Full image of the primary mirror	27
(b) Close up image of the part shown in dotted line at Figure 3.10 (a).....	28
Figure 3.11 Sag difference of the designed and fitted secondary mirror surface function.	
(a) Full image of the secondary mirror.....	29
(b) Close up image of the part shown in dotted line at Figure 3.11 (a).....	30

Figure 4.1 Components for alignment	32
Figure 4.2 Center hole blocks for alignment using ray tracing method.	
(a) Center hole block of the primary mirror.....	33
(b) Center hole block of the secondary mirror	34
Figure 4.3 MTF of the Schwarzschild-Chang type off-axis reflecting telescope which applies fabricated mirrors for various fields	36
Figure 4.4 Arrangement for a ray tracing method	39
Figure 4.5 Ray tracing process.	
(a) Incident ray from negative y	40
(b) Enlarged focus of (a).....	40
(c) Incident ray from origin.....	41
(d) Enlarged focus of (c).....	41
(e) Incident ray from positive y.....	42
(f) Enlarged focus of (e).....	42
Figure 4.6 Ascertainment of alignment using 5-hole block.....	43
Figure 5.1 Spot image of the Schwarzschild-Chang type off-axis reflecting telescope.....	45
Figure 5.2 Spot image of the off-axis reflecting telescope which uses derived surface functions.....	46
Figure 5.3 Point source test image of Schwarzschild-Chang type off-axis reflecting telescope which uses fabricated mirrors	47

List of Tables

Table 2.1 Specification of the Schwarzschild-Chang type off-axis wide-field reflecting optical system 5

Table 2.2 Tolerance analysis results of the Schwarzschild-Chang type off-axis wide-field reflecting optical system.....12

Table 3.1 Options for measurement and result of the fabricated mirror surfaces21

Table 5.1 Results of the Code V simulation and point source test46

1. Introduction

Infrared (IR) was discovered in 1800 by William Herschel. It has been used extensively for commercial and military purpose as well as for astronomical observations. In 1966, Eric E. Becklin and Gerry Neugebauer discovered an exceptionally bright IR source in the Orion Nebula which is now called the Becklin-Neugebauer Object (Neugebauer and Becklin 1971). Since their first discovery of the celestial IR source, IR observation has grown rapidly by the two infrared telescopes on Mauna Kea (Hawai'i), i.e., United Kingdom Infrared Telescope (UKIRT: United Kingdom, 3.8 m) and NASA Infrared Telescope Facility (IRTF: USA, 3.0 m), which were built in 1979.

On the other hand, the first space IR telescope, Infrared Astronomical Satellite (IRAS) was launched in 1983 (Neugebauer et al. 1984). After that, many satellites for infrared observation succeed their projects (see the reviews by Glass 1999), e.g., Infrared Space Observatory (ISO) in 1995 (Kessler et al. 1996), Space Infrared Telescope Facility (SIRTF) in 2002 (Fanson et al. 1998), and AKARI which was launched under the name ASTRO-F in 2006 (Murakami et al. 2007). These days, three biggest next-generation space infrared telescopes are currently planned, i.e., James Webb Space Telescope (JWST: Clampin 2008), Herschel Space Observatory (HSO: Tofani and Natale 2003) and Space Infrared Telescope for Cosmology and Astrophysics (SPICA: Nakagawa and Murakami 2007).

For IR telescopes and instruments, it is difficult to make the optical system using refractive lens components, because refracting optical system has unavoidable chromatic aberration and absorptions in IR band. In addition, large-size lens for the refracting optical system is difficult to fabricate and to mount (Lee 1992). In the Infrared wavelength range, design employing reflectors are preferable to avoid chromatic aberrations and absorption in a refractive lens system.

The conventional on-axis reflecting telescope, however, has deficiencies in the imaging quality. Obstruction of the secondary mirror causes scattering, diffraction and stray light (Chang 2006; Moretto and Kuhn 2000; Moretto et al. 2004). The scattered light causes two problems: (1) enhanced photon noise due to the excessive scattered light; and (2) time variable systematic noise due to a complicated point Spread Function (PSF) of the telescope (Kuhn and Hawley 1999). Measurements requiring very wide photometric dynamic range (like astronomical observations of faint objects near bright sources such as extra-solar planet detection) are often limited by the scattered light characteristics of the telescope (Moretto et al. 2004). In addition, the obstruction imposes restrictions on wide field of view (FOV) which required a large size secondary mirror (Moretto and Kuhn 1999). In nowadays several off-axis reflecting telescope projects are currently on-going, e.g., New Off-axis 1.7 m Solar Telescope (NST; Didkovsky et al. 2004) and Advanced Technology Solar Telescope (ATST; Keil et al. 2003).

Aberration theory to design off-axis optical systems has been relatively undeveloped until lately. As a result, most existing off-axis telescope designs are using eccentric sections of the on-axis parent telescope. Recently, a geometrical aberration theory dedicated for classical off-axis reflecting telescopes and imaging systems has been developed (Chang and Prata 2005; Chang et al. 2006). A simple closed-form equation of this theory can eliminate linear astigmatism which is the dominant aberration of classical off-axis two-mirror systems. Furthermore, it was shown that the geometric optical performance of a classical off-axis two-mirror system without linear astigmatism is equivalent to that of a conventional classical two-mirror on-axis telescope (Chang 2006).

Off-axis aspheric mirrors are manufactured in two different methods. In the first way, a small part of the conic section is cut from a large aspheric mirror. In this configuration the back surface of the off-axis aspheric mirror is approximately perpendicular to the side surface and to the optical axis. In the second way, an off-axis aspheric mirror is directly manufactured as an off-axis segment. In this case, there is no relation between the back surface and the optical axis (Lee 1992). The fabrication of asymmetric off-axis mirror had

been impossible until lately so people used some parts of conic sections. But manufacturing of non-axially-symmetric optical elements is no more formidable, by advances of diamond turning machine technology (Kim et al. 2007; Yang et al. 2007).

The biggest problem of the off-axis reflecting telescope is difficulty in alignment. Because the alignment of an off-axis reflecting telescope requires more degrees of freedom (DOF) than an on-axis reflecting telescope. Classical off-axis reflecting telescopes are aligned using interferometer method and Hartmann test. Since the alignment tolerance of the infrared telescope is much larger than that of the optical wavelength, the interferometer methods using optical laser beam is not suitable to our system. We develop the alignment system based on a ray tracing method.

In this thesis, we present a development of the infrared wide-field off-axis reflecting telescope. In section 2, we describe optical design and specification of the Schwarzschild-Chang type off-axis reflecting telescope. In section 3, we explain the fabrication, measurement and analysis of the off-axis mirrors. In section 4, we describe the alignment process of telescope system. In section 5, we present the result of point source simulation and measurement.

2. Design and tolerance analysis

2.1 The Schwarzschild-Chang reflecting telescope

In this work, we made a wide-field off-axis reflecting telescope base on the Schwarzschild-Chang type that has similar concept with Inverse Cassegrain type (Chang 2006). In Figure 2.1, the primary mirror spreads rays that come from source and the secondary mirror concentrates spread rays to a focal plane. The Schwarzschild-Chang type off-axis reflecting telescope has short effective focal length (EFL) compare with entrance pupil diameter (EPD) for the wide-field (see Table 2.1). Secondary mirror is designed bigger than primary mirror to minimize aberrations like coma and astigmatism. Pixel size of the detector is 50 μm and the limit resolution of the detector is 11 cycle/mm. The surfaces of primary and secondary mirror are represented by polynomial form like Equation 1.

$$z(x,y) = a_0x + a_1y + a_2x^2 + a_3xy + a_4y^2 + a_5x^3 + a_6x^2y + a_7xy^2 + a_8y^3 + a_8x^4 + a_9x^3y + a_{10}x^2y^2 + a_{11}xy^3 + a_{12}y^4 + \dots + a_{64}y^{10} \quad (1)$$

The Schwarzschild-Chang type off-axis reflecting telescope has wide FOV. Images are changing at the each field because of aberrations (see Figure 2.2). The MTF (Modulate Transfer Function) is more than 70 % at the limit resolution of a detector for 10 μm wavelength (see Figure 2.3).

Parameter	Value
Diameter of primary mirror	70 mm
Diameter of secondary mirror	130 mm
EFL (Effective Focal Length)	100 mm
Aperture	50 mm
Pixel size of detector	50 μm
Pixel FOV of detector	100 "
FOV of array (256 \times 256)	7.1 \times 7.1 degrees
Wavelength coverage	8 - 12 μm

Table 2.1 Specifications of the Schwarzschild-Chang type off-axis wide-field reflecting optical system.

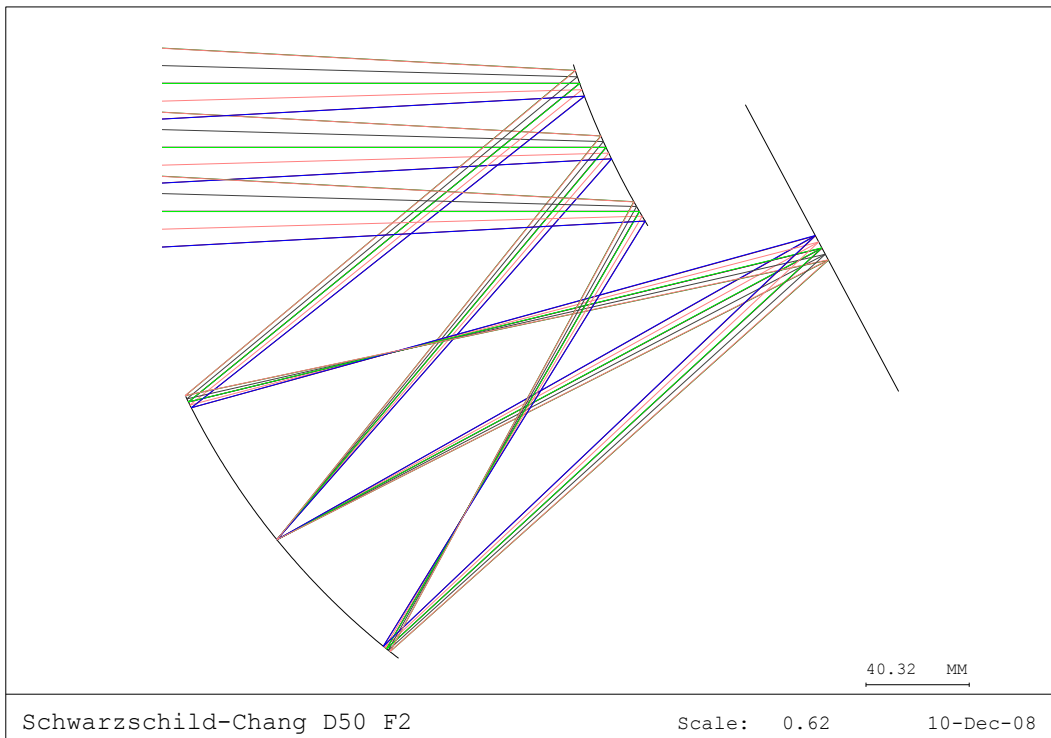


Figure 2.1 Layout of the Schwarzschild-Chang type off-axis reflecting telescope.

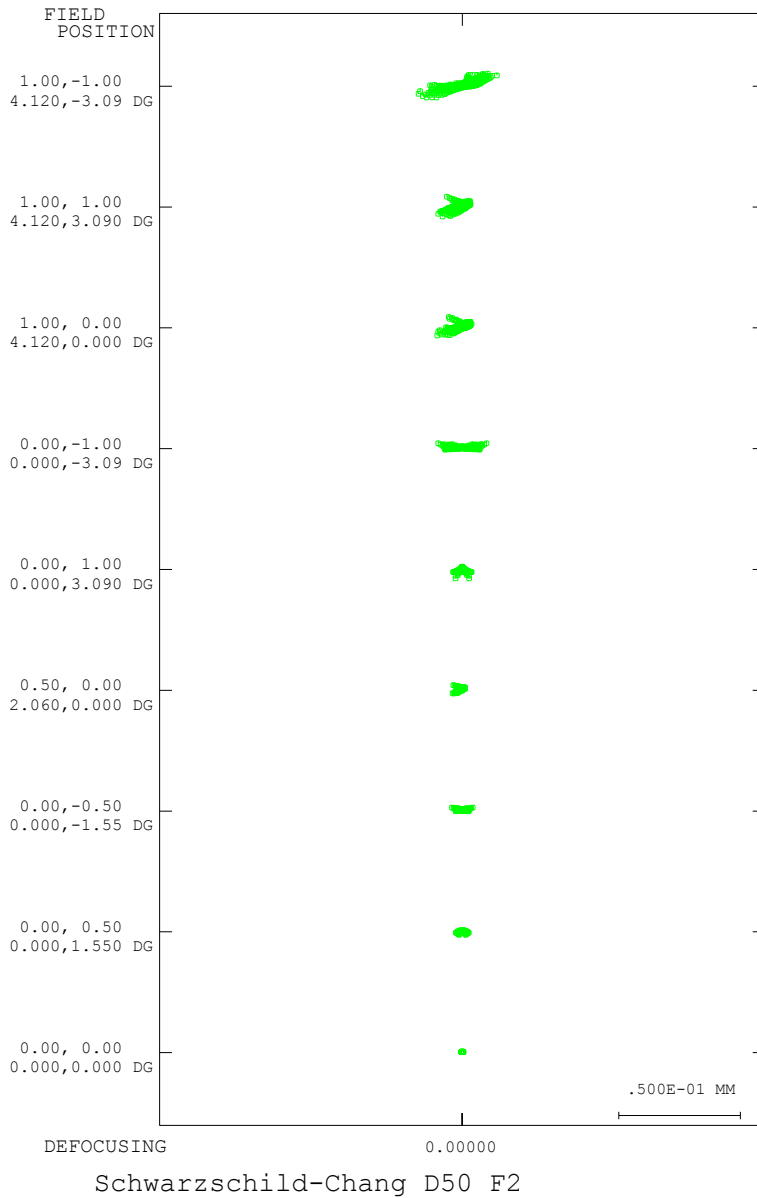


Figure 2.2 Spot diagram of the Schwarzschild-Chang type off-axis reflecting telescope for various fields. Spot diagram in Code V does not consider the diffraction limit.

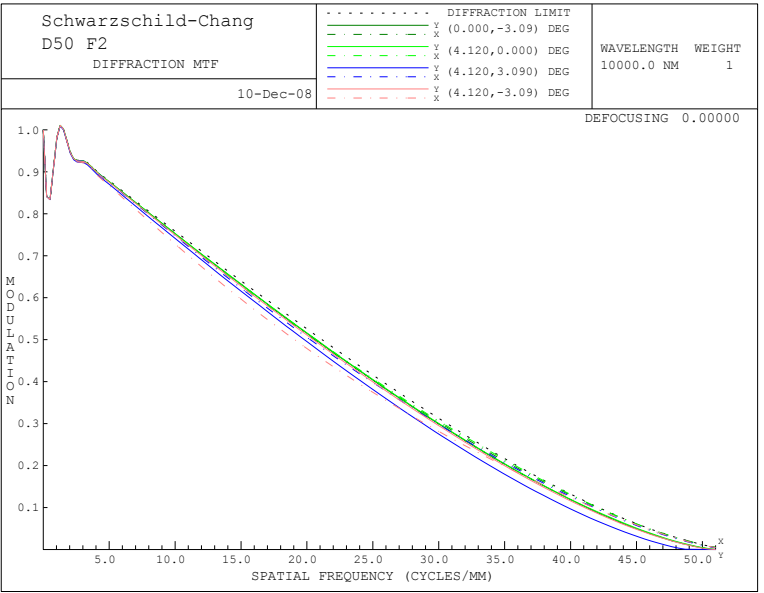
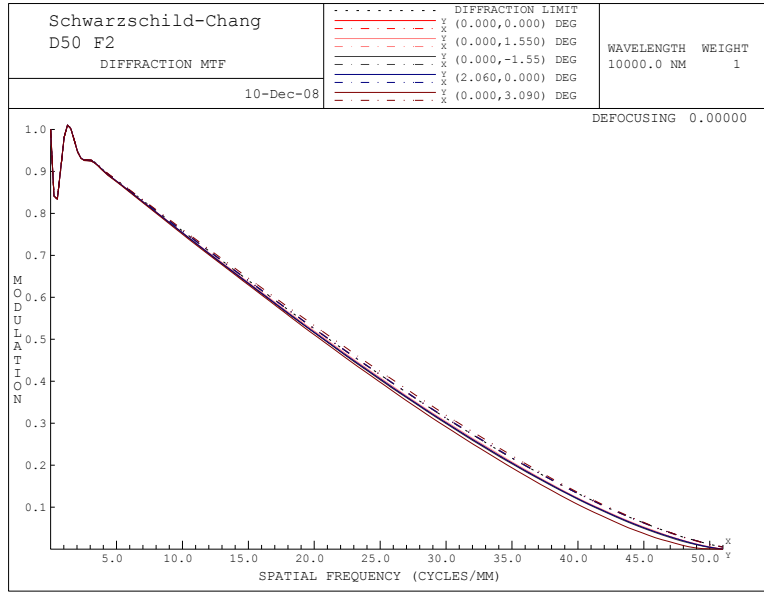


Figure 2.3 MTF of the Schwarzschild-Chang type off-axis reflecting telescope for various fields. Code V support two analysis modes for MTF. First one is geometrical analysis mode that does not consider diffraction limit and another one is diffraction mode. Top and bottom of Figure 2.3 graphs are diffraction mode MTF for 10 μm wavelength.

2.2 Tolerance analysis.

We use the Code V* for the tolerance analysis of the Schwarzschild-Chang type off-axis reflecting telescope. Spot diagram which is one of analysis option in Code V does not consider diffraction limit. So we use encircled energy analysis for tolerance analysis and 84% Encircled Energy Diameter (EED) is equivalent to spot diameter. Airy disk size is defined diameter of encircled energy which includes the 84 % of the total energy and given by

$$\text{Size of Airy Disk} = 2.44 \cdot \lambda \cdot \frac{F}{D} \quad (3)$$

where F is effective focal length, D is Aperture of telescope and λ is the wavelength of the light (Lena 1988). Airy disk size of the reflecting telescope which has same f-ratio with our telescope is 49 μm for 10 μm wavelength. For 10 μm wavelength, 84% Encircled Energy diameter of Schwarzschild-Chang type off-axis reflecting telescope is 51 μm at the center of the image.

We conducted tolerance analysis in Code V and compensated image quality by changing back focal length (BFL) that is distance between secondary mirror and image plane in z-axis. A compensator, in our case is BFL, is a construction parameter that can be adjusted to compensate for an error introduced by another construction parameter (Bass 1995). Tolerance analysis carried out for despace, decenter and tilt tolerance (see Figure 3.1). Despace is defined displacement of the secondary mirror toward or away from the primary mirror in z-axis. Decenter is defined error in position of the secondary mirror in x and y axes. We did not consider z-axis for decenter because decenter of z-axis is eliminated by compensator. Alpha (α)-, beta (β)- and gamma (γ)- tilts are defined each rotations of x, y and z axis (Schroeder 2000).

For tolerance analysis, the range of tolerance is determined by the size of 84% EED when that is under 90 μm . As the results of tolerance analysis, despace has the largest tolerance range.

* Code V is the optical design and simulation program of Optical Research Associates (ORA).

The critical tolerance is α -tilt of the secondary mirror (see Table 3.1). And we ascertain that tolerances of the tilt are tighter than tolerances of the position when the off-axis reflecting telescope is assembled and fabricated. So we should pay special attention to adjusting tilt angles of off-axis mirrors.

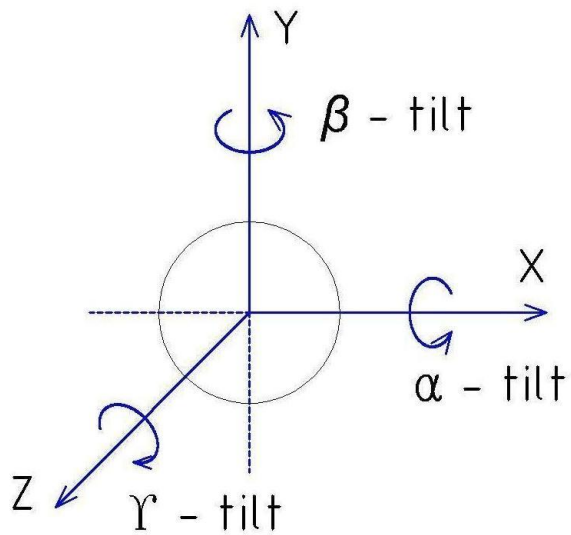
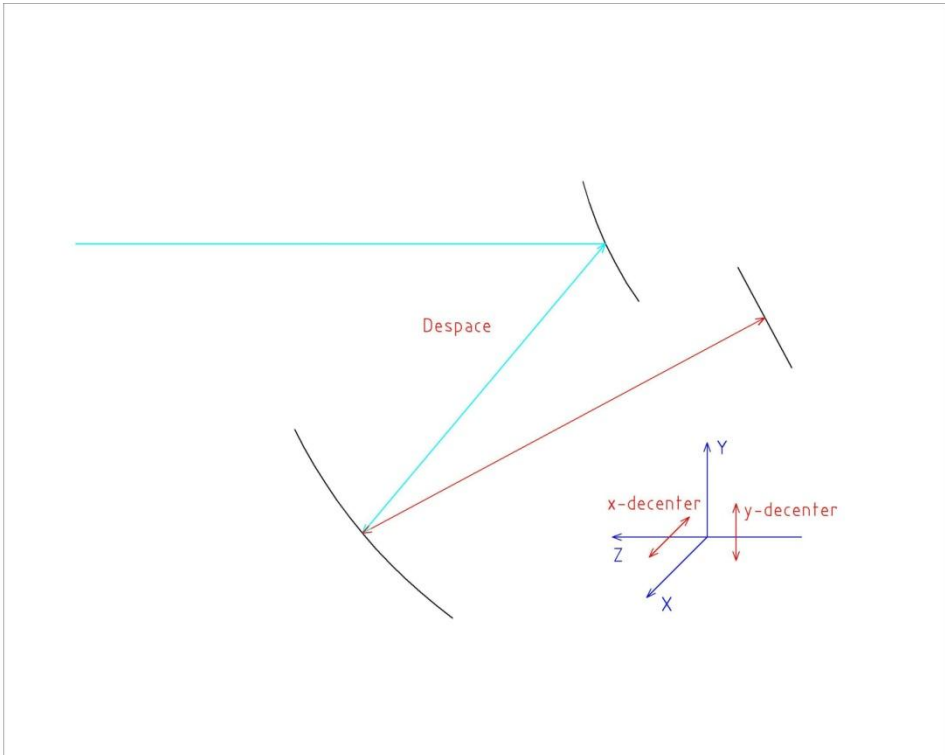


Figure 2.4 Tolerances of the Schwarzschild-Chang type off-axis reflecting telescope. Top of the image is tolerance by positional error. Bottom of the image is tolerance by angular error.

Tolerance	Value	Size of 84 % EED [μm]
Despace	- 3.0	84
	+ 3.0	84
Decenter of x-axis	- 0.5	85
	+ 0.5	85
Decenter of y-axis	- 0.5	86
	+ 0.5	85
Primary α -tilt	- 0.2	82
	+ 0.2	82
Primary β -tilt	- 2.0	82
	+ 2.0	82
Secondary α -tilt	- 0.09	88
	+ 0.09	87
Secondary β -tilt	- 0.1	84
	+ 0.1	84

Table 2.2 Tolerance analysis results of the Schwarzschild-Chang type off-axis wide-field reflecting optical system. Size of 84 % EED is compensated for changing BFL. The unit of the despace and decenter is mm and unit of the tilt is degree.

3. Fabrication of off-axis mirrors

3.1 The backside structure of the off-axis reflecting mirrors

The biggest problem of Schwarzschild-Chang type off-axis reflecting telescope is difficulty in alignment, because primary and secondary mirrors do not share the same optic axes. And also the off-axis reflecting telescope has gamma-tilt tolerance which is not the same as an on-axis reflecting telescope. So our system adopted four pins and pin holes on the commissure of mirrors and stages to minimize the stages and mirrors assembling errors like gamma-tilt and decenter of mirrors (see Figure 3.1 and 3.2).

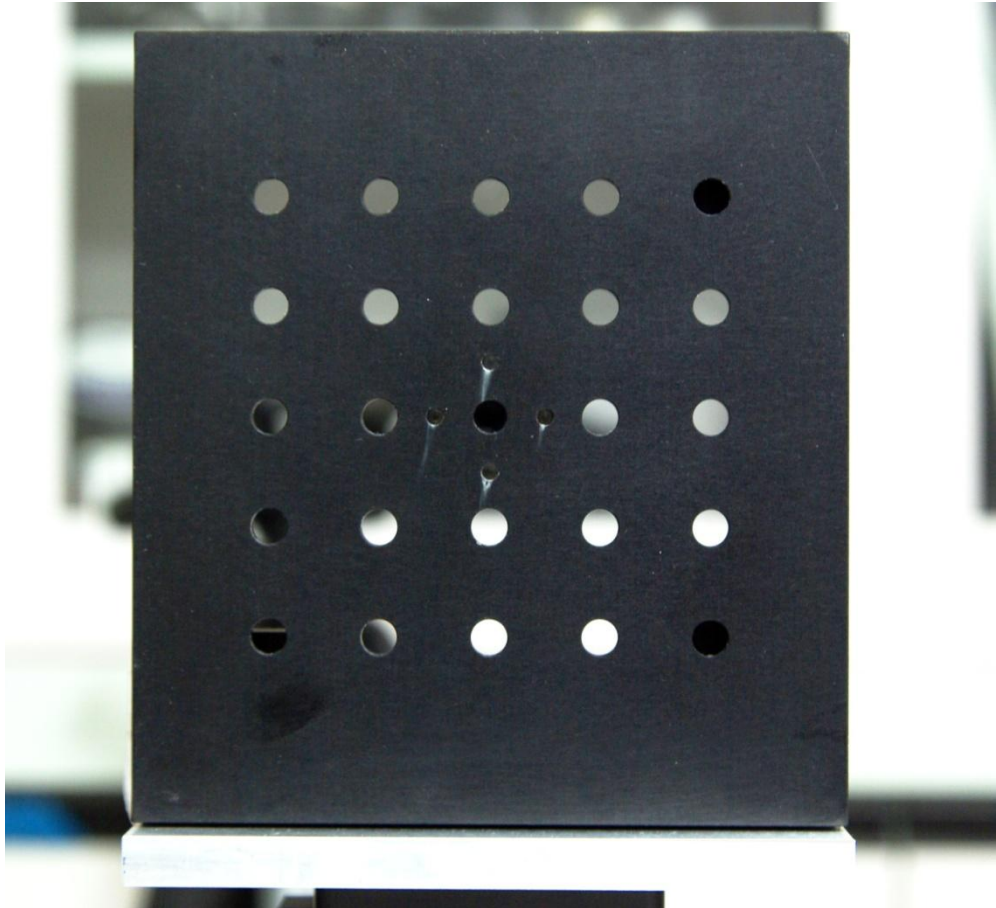


Figure 3.1 Secondary mirror stage. Primary and secondary mirror stages have 4 pin holes. Small holes at the center of the stage are pin holes. Stages can regulate x-, y- and z- axes and we can also control α - and β -tilts.

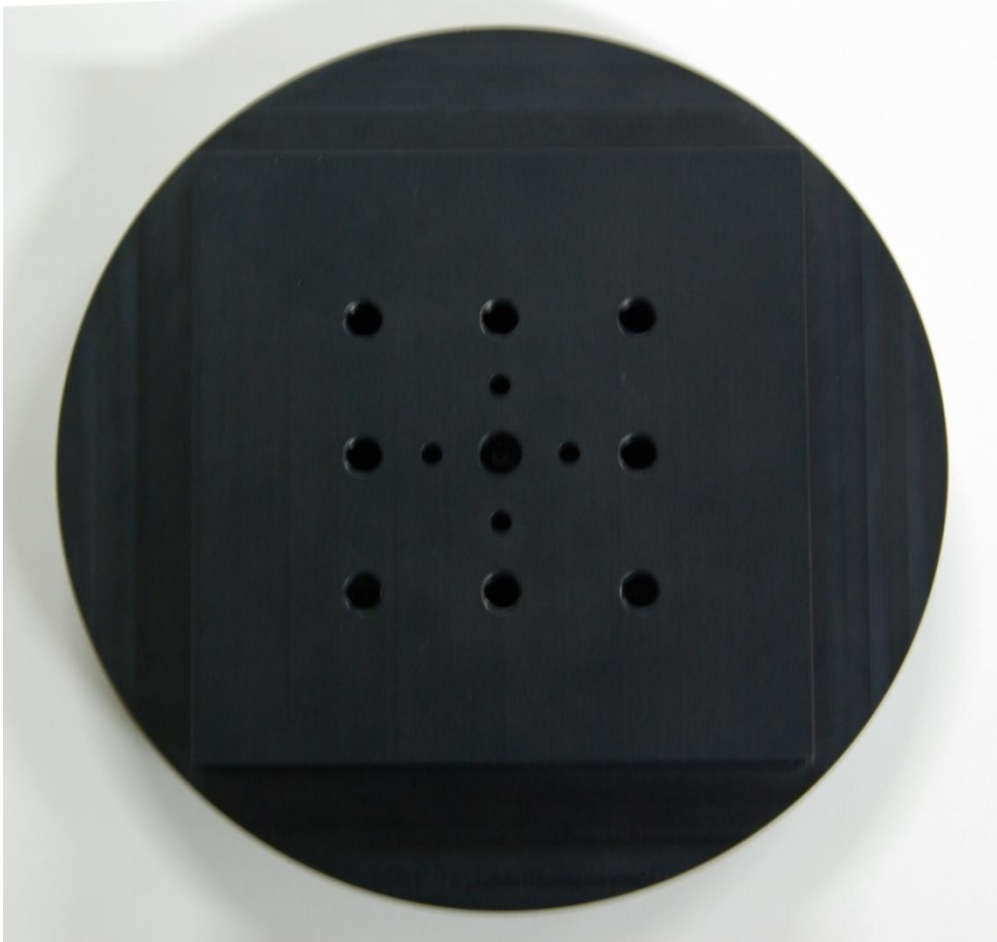


Figure 3.2 Backside structure of the secondary mirror. There are two kinds of holes at the backside of mirrors. The small holes are pin holes to minimize the assembling errors. Another holes are tap for assemble.

3.2 Machining off-axis reflecting mirrors

The off-axis reflecting mirrors were made from aluminum (Al6061-P6). First, we fabricated spherical mirrors which have less than 0.2 mm difference with designed surface functions to minimize machining time. After that, we fabricated the off-axis mirrors by diamond turning machine (DTM) Freeform 700A (Precitech, Inc.) which is shown in Figure 3.3. Freeform 700A is 5-axis control ultra precision diamond turning machine and we control three axes and aerostatic spindle to rotate the mirror substrate, and X-axis linear servo floating on a hydrostatic bearing to laterally move the spindle together with the mirror, and a Z-axis linear hydrostatic servo to translate the diamond tool for generate depth profile (Kim 2007). Rotation of the C axis is controlled by low speed, about 50 RMP, because we control the tree axes to synchronize the spin of C-axis and position of diamond bite. The details of the mechanical structure will be discussed in Yang et al. (2009).



Figure 3.3 Machining image of the primary mirror. Off-axis primary mirror is manufactured by Freeform 700A. The nozzle which is under the diamond bite ejects mist (oil + air) to eliminate chips easily.

3.3 Measurement of off-axis reflecting mirrors

Surface roughness of fabricated off-axis reflecting mirrors (see Figure 3.4 and 3.5) was measured by optical surface profilometer (NT 2000, Wyko Inc.). Local surface roughness of primary and secondary mirrors are Ra 4.21 nm and Ra 4.24 nm, where Ra means the center line average of surface roughness. We check the two values of form accuracy. First one is peak-to-valley (P-V) and P-V defined the maximum departure of the actual difference from the desired mirror surface in both positive and negative directions. Another one is root mean square value of the difference between designed surface function and fabricated mirror surface, called RMS. P-V is easily influenced by vibration, scratch or mote. So we usually use RMS value to estimate the quality of the fabricated one (Kim 2003). Form accuracy of fabricated off axis reflecting mirrors were measured using ultrahigh accurate 3-D profilometer (UA3P, Panasonic Corp.) which uses the atomic force probe (AFP) for measurement. UA3P makes AFP approach to the territory where repulsive atomic force generates against the measurement surface and always keeps the atomic force constant. As that reason, UA3P can measure the object without concerning the reflectance of the measurement surface (Tsutsumi 2005). Measurement data of primary and secondary mirrors are at the Table 3.2.

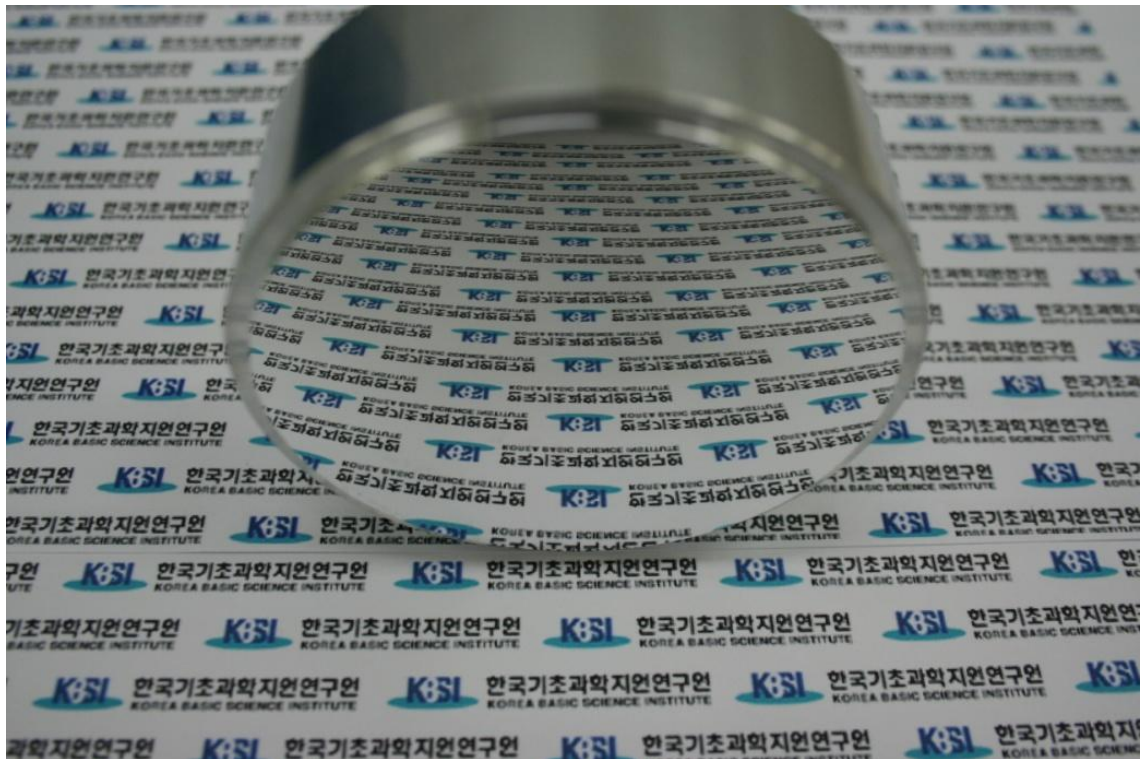


Figure 3.4 Primary mirror of the off-axis reflecting telescope.

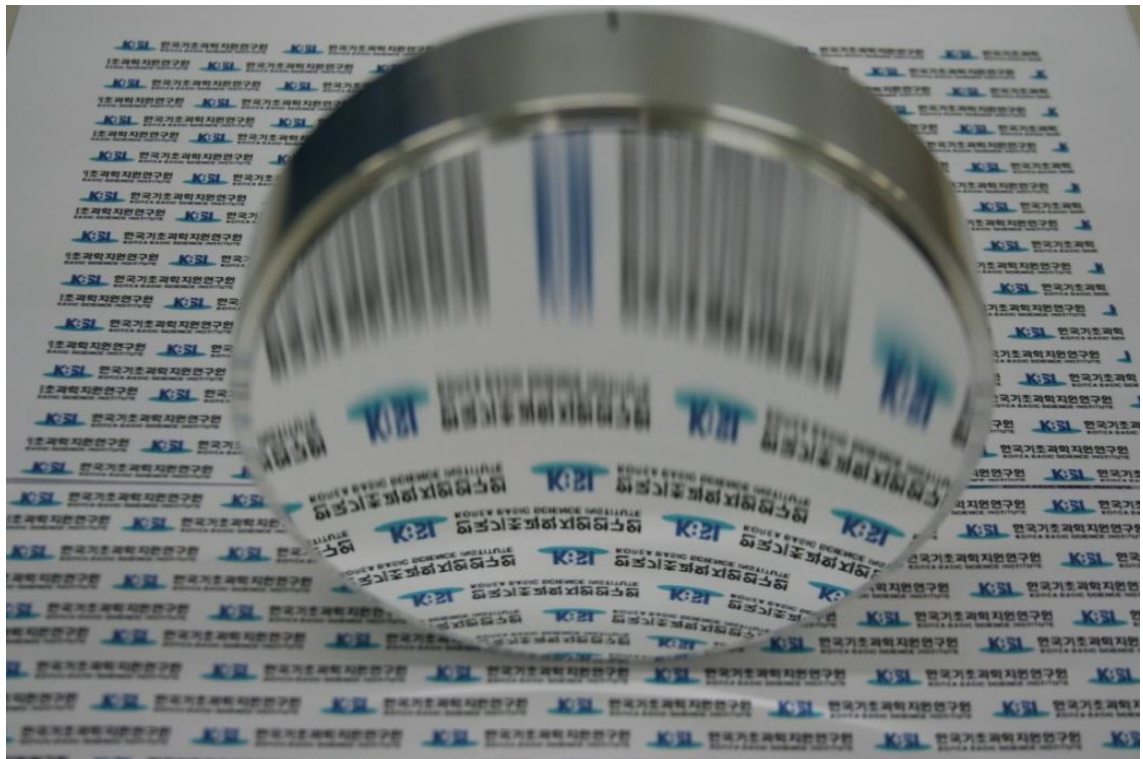


Figure 3.5 Secondary mirror of the off-axis reflecting telescope.

Item	Primary	Secondary
Probe radius	1.3 μm	1.3 μm
Measurement pitch of x-axis	10.0 μm	10 μm
Measurement pitch of y-axis	10.0 μm	10 μm
Measurement speed of x-axis	2.0 mm/sec	2.0 mm/sec
Measurement speed of y-axis	- 2.0 mm/sec	- 2.0 mm/sec
Number of measured points	62114	217516
P-V	0.87 μm	3.1 μm
RMS	0.19 μm	0.72 μm

Table 3.2 Options for measurement and result of the fabricated mirror surfaces. The probe move along the \square shape path.

3.4 Numerical format of the measured mirror surfaces

To analyze the fabricated mirrors, we made fitted surface functions that represent surfaces of fabricated mirror surfaces (see Figure 3.8 and 3.9) using measured data of the fabricated mirror surfaces. We used MPFIT_2D in interface description language (IDL) for fitting and the form of new polynomial is the same as designed form (see Figure 3.6 and 3.7). MPFIT** is generally more stable and less likely to crash than the brute-force approach taken by CURVEFIT, which is IDL routine based upon numerical recipes. So, MPFIT has additional capabilities not found in CURVEFIT and these IDL routines provide a robust and relatively fast way to perform least-squares curve and surface fitting.

The surface functions that are derived by IDL are applied to our system in Code V. The performance of the off-axis reflecting telescope which uses fitted surface functions is optimized by changing BFL. To fit the surface function of the primary mirror, MPFIT_2D operate interpolation 10 times. The sag difference of the derived surface function and the measured data of the fabricated primary mirror is RMS $0.27 \mu\text{m}$. To fit the surface function of secondary mirror, MPFIT_2D operate interpolation 25 times. The sag difference of the derived surface function and the measured data of the fabricated secondary mirror is RMS $0.37 \mu\text{m}$. Even though the periphery on the fitted mirror surfaces are off by hundreds of nanometers from the designed shapes, the derived surface areas in the central parts agree well with those of the optical design (see Figure 3.10 and 11).

** MPFIT: Markwardt; homepage: <http://cow.physics.wisc.edu/~craigm/>

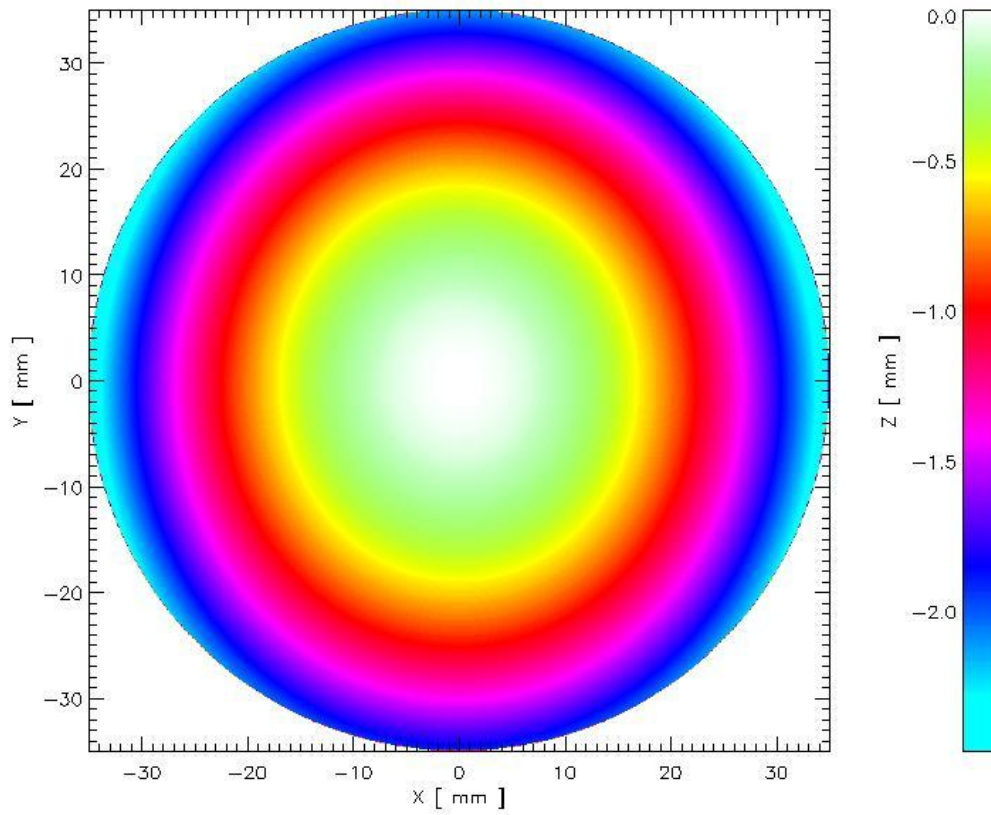


Figure 3.6 Intensity map of the designed primary mirror surface function.

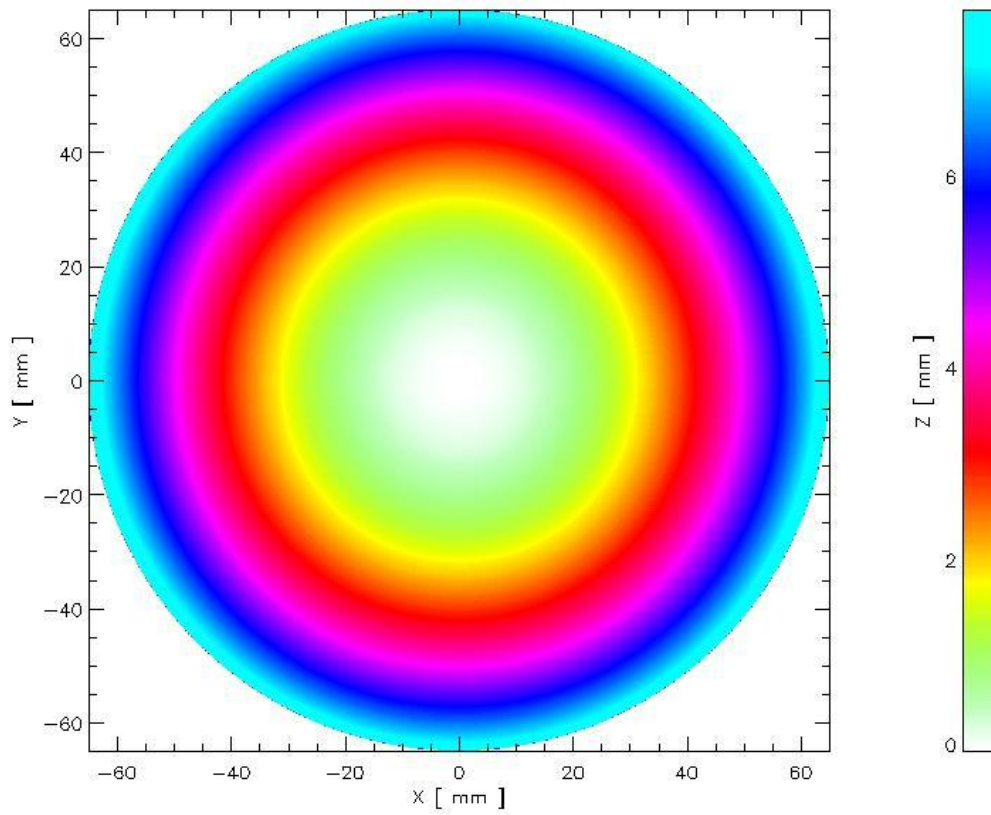


Figure 3.7 Intensity map of the designed secondary mirror surface function.

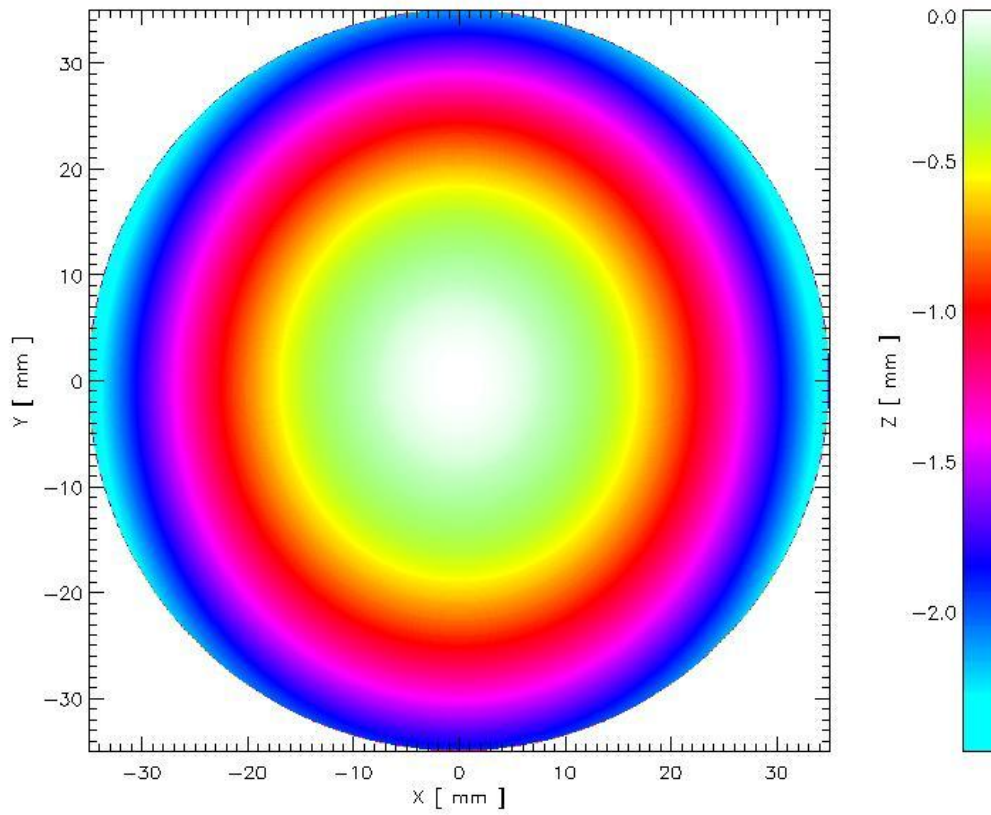


Figure 3.8 Intensity map of the fitted primary mirror surface function.

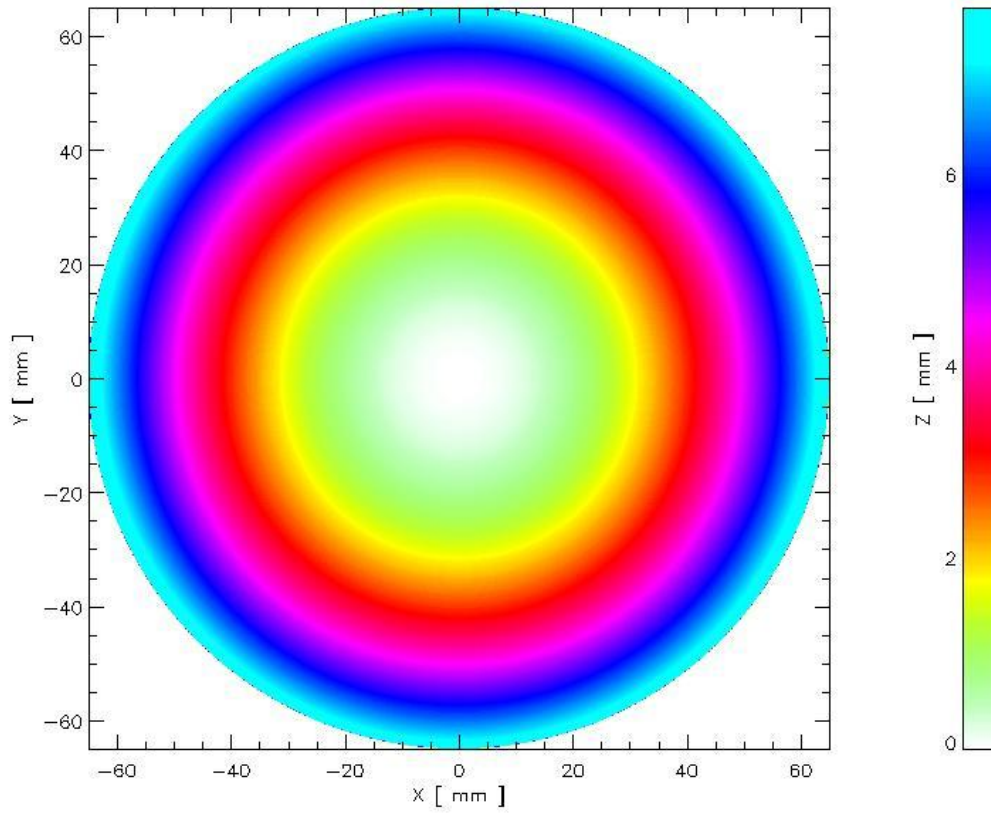
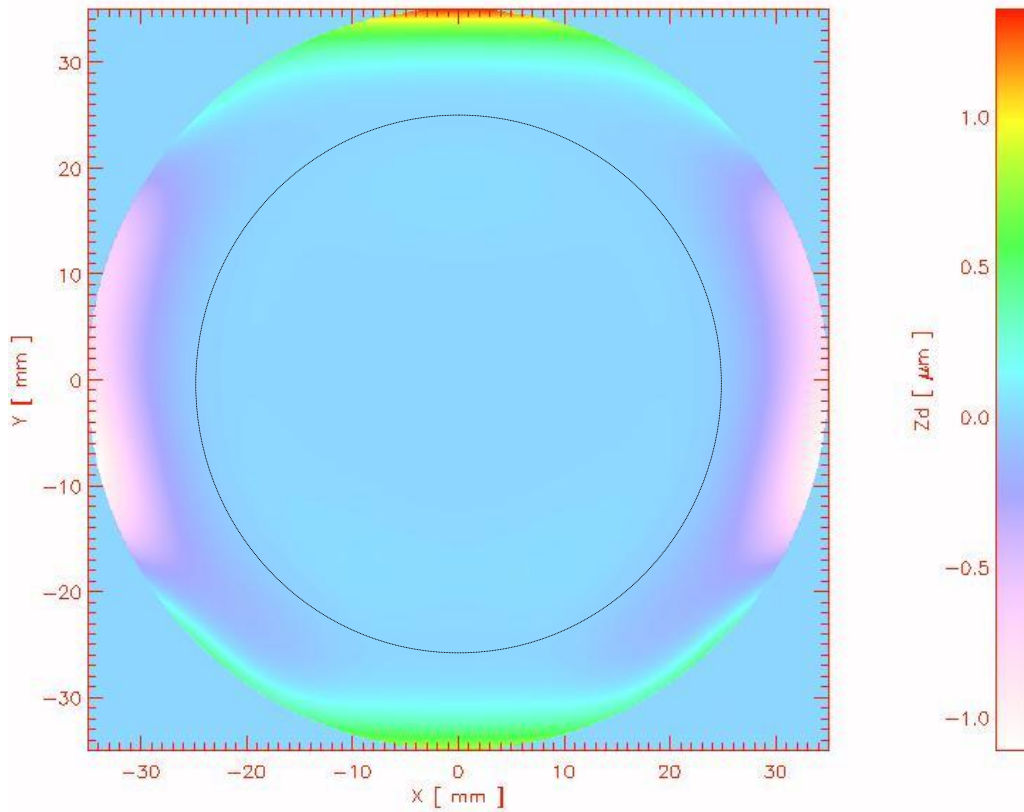
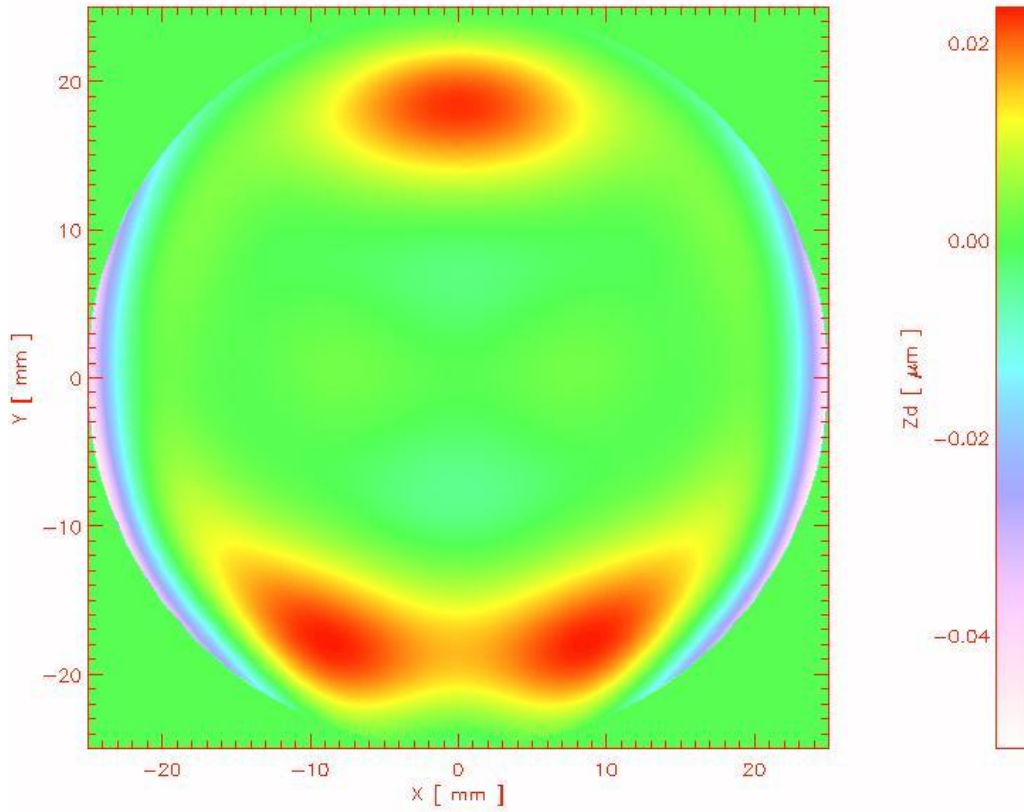


Figure 3.9 Intensity map of the derived secondary mirror surface function.



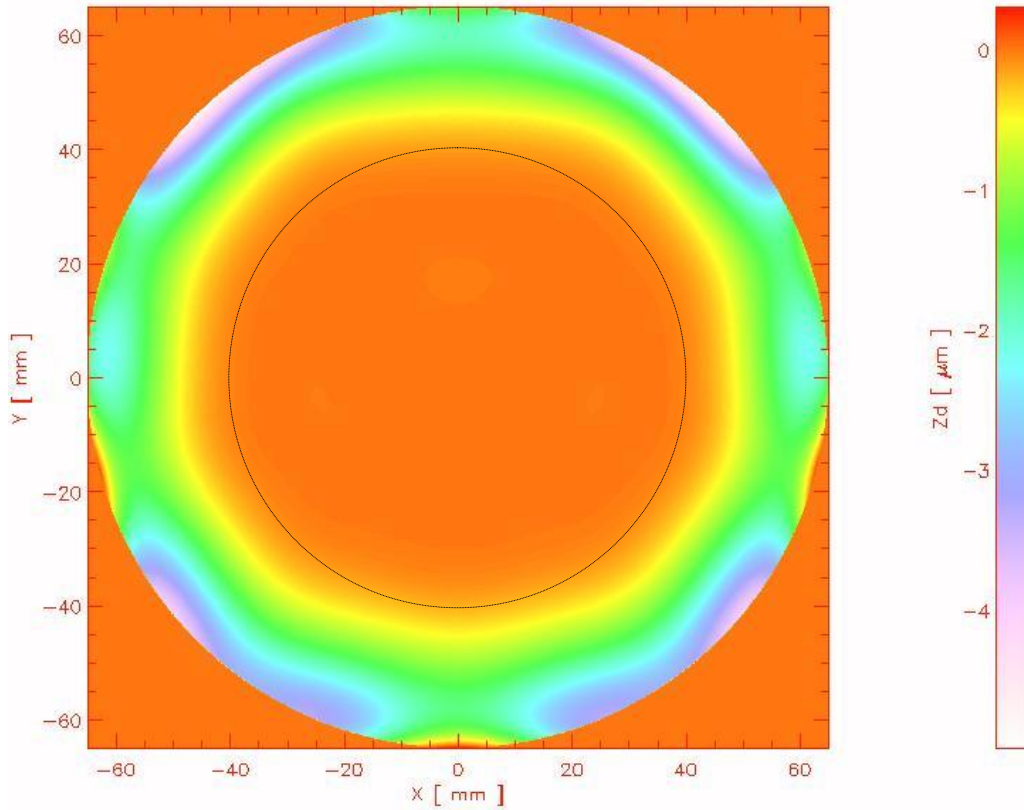
(a)

Figure 3.10 Sag difference of the designed and fitted primary mirror surface function. (a) Full image of the primary mirror.



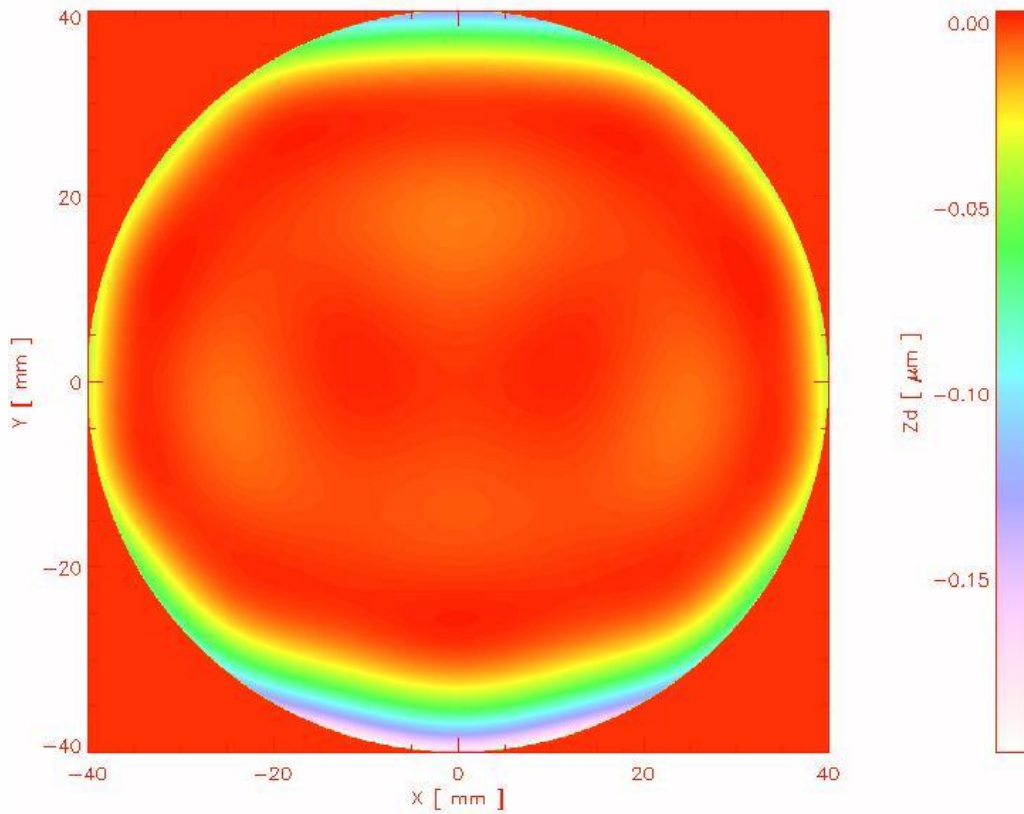
(b)

Figure 3.10 (b) Close up image of the part shown in dotted line at Figure 3.10 (a).



(a)

Figure 3.11 Sag difference of the designed and fitted secondary mirror surface function. (a) Full image of the secondary mirror.



(b)

Figure 3.11 (b) Close up image of the part shown in dotted line at Figure 3.11 (a).

4. Alignment system of off-axis telescope

4.1 Manufacturing of the alignment system

To align the Schwarzschild-Chang type off-axis reflecting telescope, we used laser pointer (laser diode, 632.8 μm wavelength) for ray tracing method based on the geometrical optics. Alignment of telescope was conducted on the optical table. Some components are used for ray tracing, i.e., a stop, a 5-hole block, a primary mirror center hole block, a secondary mirror center hole block and a flat mirror (see Figure 4.1 and 4.2). We fabricated base blocks for each stage. Because primary mirror, secondary mirror and detector are not parallel to optic axis (see Figure 4.1).

After calibration of the stages position, stages are assembling with primary, secondary and flat mirrors. We made parallel ray which traces the center of the primary mirror by adjusting tilt and translation of laser pointer. Because, the parallel ray of the laser pointer is not perfect, we set up the pin hole in front of the laser pointer. Based on the geometrical optics, all parallel rays which trace the optical path of telescope should be focused on one point irrespective of incidence position of rays.

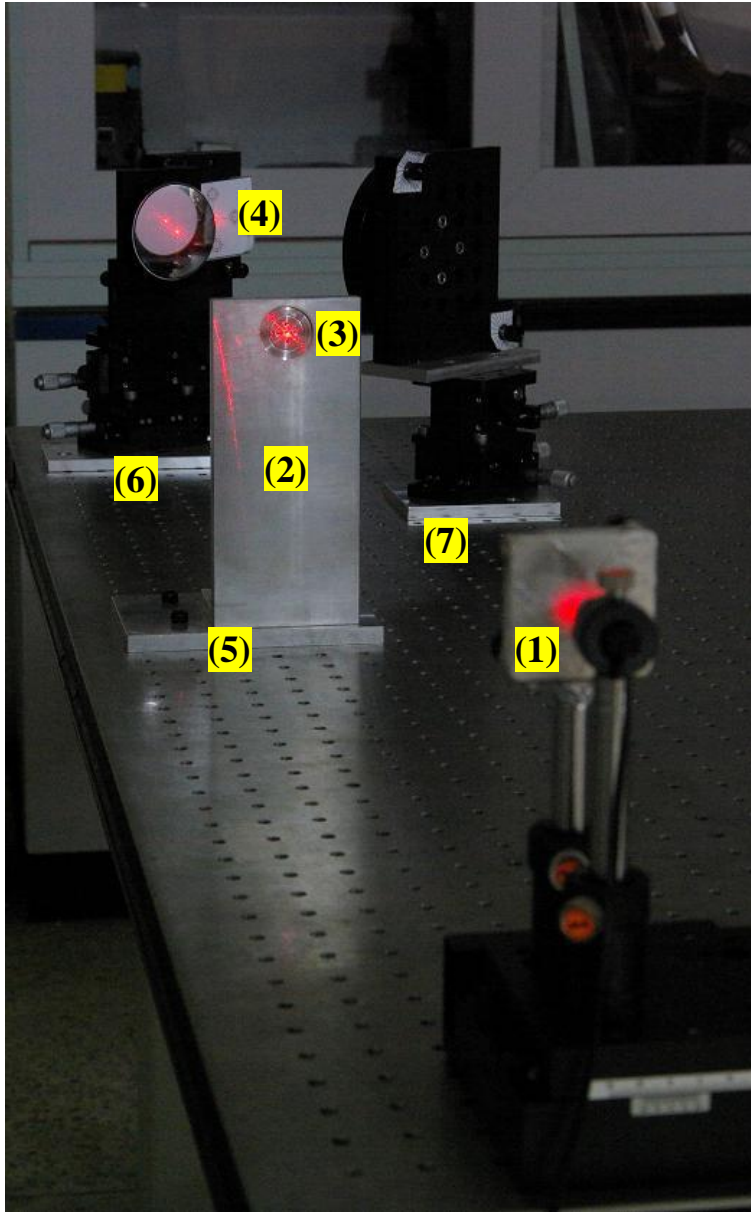
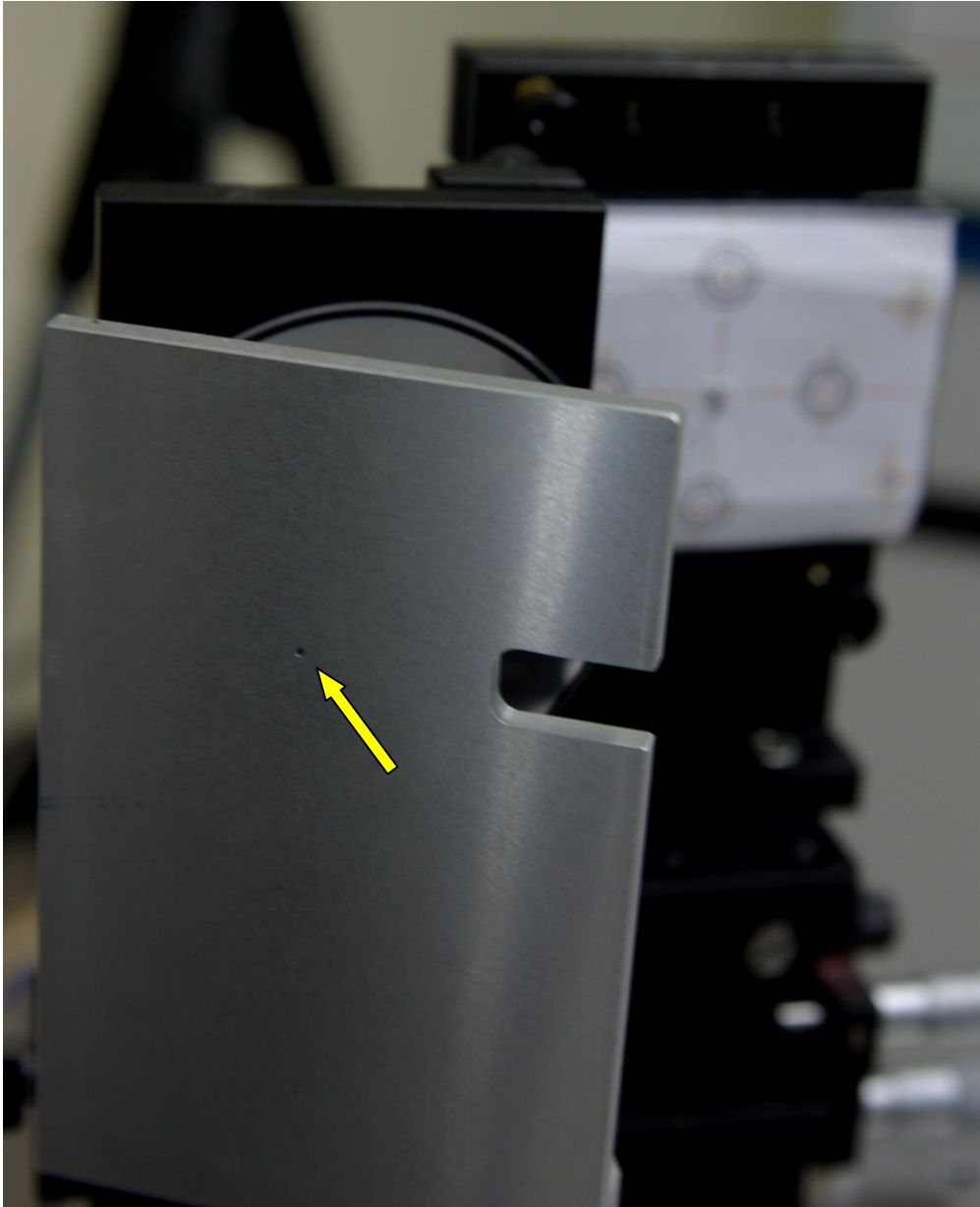
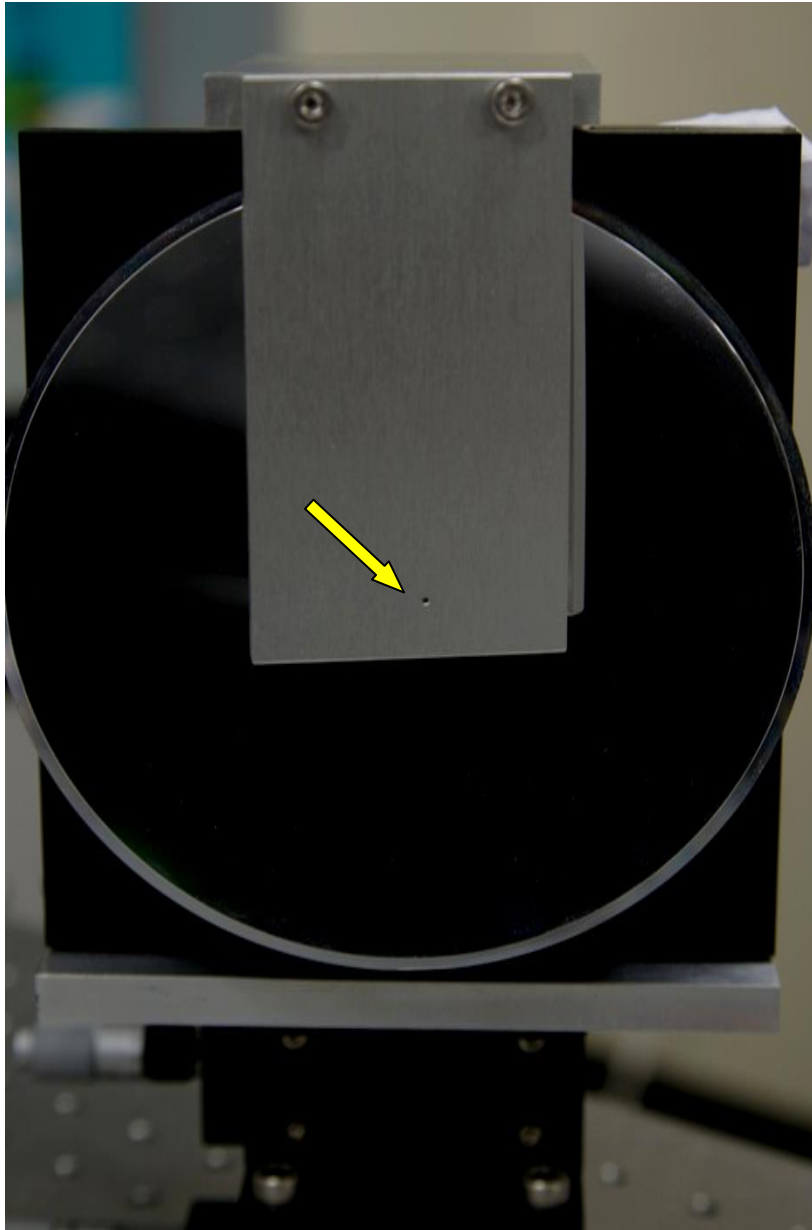


Figure 4.1 Components for alignment. (1) is a source, (2) is a stop, (3) is a 5-hole block, (4) is a flat mirror and (5 - 7) are base blocks of each mirror.



(a)

Figure 4.2 Center hole blocks for alignment using ray tracing method. (a) Center hole block of the primary mirror. The diameter of the hole is 1 mm. The opening which located at the right side of block is the way to clear the incident ray.



(b)

Figure 4.2 (b) Center hole block of the secondary mirror. The secondary mirror center hole block is composed block and support.

4.2 Optimization and tolerance analysis using fitted mirrors

We compared the performance of the Schwarzschild-Chang type off-axis reflecting telescopes with off-axis reflecting telescopes which uses the derived surface functions (see section 3.4). Performance of MTF is deteriorated from 70 % to 50 % and the EED is enlarged from 51 μm to 116 μm for the 10 μm wavelength (see Figure 4.3).

We conducted tolerance analysis about the off-axis telescope which uses the fitted surface functions. Range and sort of tolerances are the same as the tolerance analysis of the Schwarzschild-Chang type off-axis reflecting telescope (see Table 2.2). Comparing the off-axis reflecting telescope which uses the fitted surface functions with the designed off-axis reflecting telescope, the most ineffective tolerance for the two telescopes is despace. On the other hand, the most sensitive tolerance is not same. The most sensitive tolerance of the designed off-axis reflecting telescope is α -tilt of the secondary mirror but positive y-axis decenter is the most sensitive tolerance of the off-axis reflecting telescopes which uses the designed surface functions.

We ascertained that tolerances are not dominant to the quality of the off-axis reflecting telescopes which applied fitted surface function as compared with the designed off-axis reflecting telescope. And also, EED of each field have a shade difference. Furthermore some tolerances, like negative y-axis decenter and clockwise secondary mirror's alpha tilt, improve the image quality of the off-axis reflecting telescope which uses the derived surface functions, because we optimize that changing BFL and freezing the other variables.

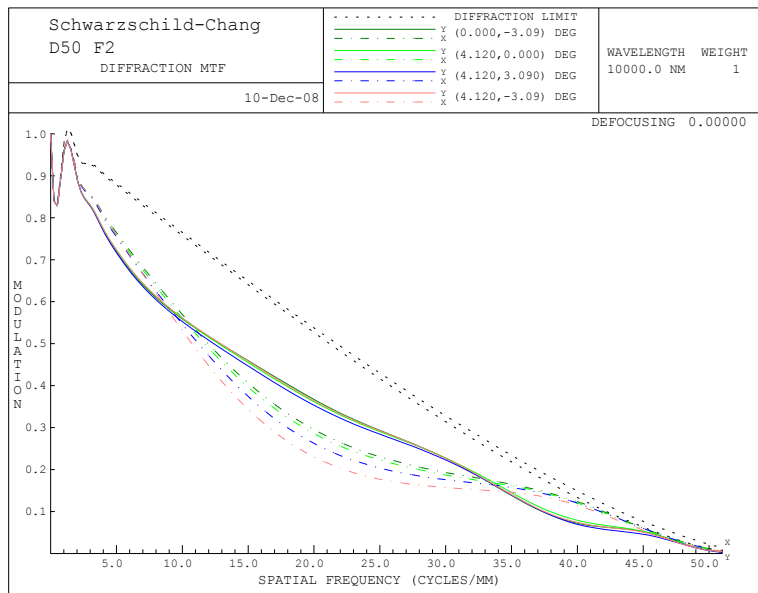
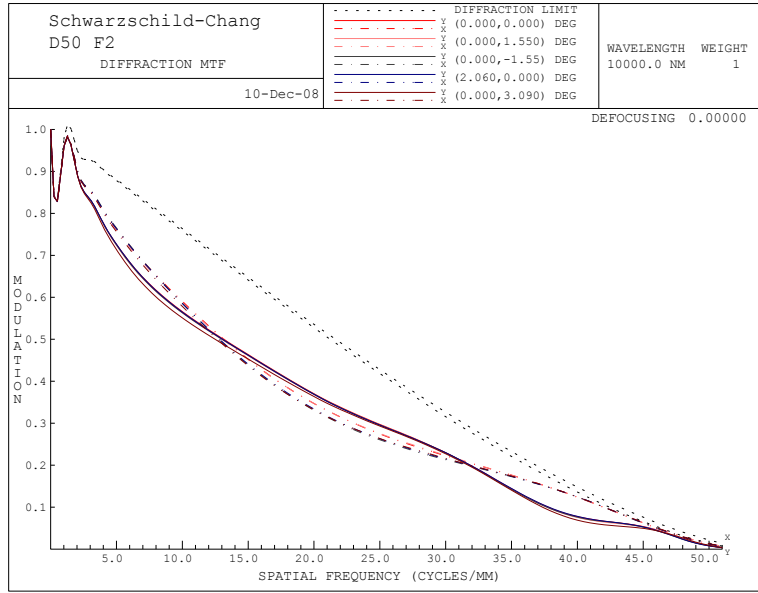


Figure 4.3 MTF of the Schwarzschild-Chang type off-axis reflecting telescope which applies fabricated mirrors for various fields. Top and bottom of figure 3.9 graphs are diffraction mode MTF for 10 μm wavelength.

4.3 The ray tracing method for alignment

The ray tracing method for alignment is as follows (see Figure 4.4 and 4.5):

1. Assemble the components, i.e., laser pointer, stop and base blocks to the optical table.
2. Assemble the mirror stages to each base block.
3. Assemble primary, secondary and flat mirrors to the each stage.
4. Calibrate position of each mirror stage.
5. Set up the laser pointer and stop.
6. Assemble the center hole blocks of primary and secondary mirror in front of each mirror stage.
7. Calibrate the laser pointer to the incident ray from the laser pointer through the center of 5-hole block.
8. Regulate the α - and β -tilt of the primary mirror stage until the ray which entered from the center of the primary mirror focus to the center of secondary mirror.
9. Regulate the alpha and beta tilt of the secondary mirror stage until the ray which entered from the center of the secondary mirror incident to the center of flat mirror.
10. Regulate the alpha and beta tilt of the flat mirror stage until the ray return back to the entered light path after reflected by flat mirror.
11. Shifted the stage of laser pointer to positive x direction. We ascertained that the focus does not move.
12. We conducted same process for negative x, and $\pm y$ direction and ascertained that focus does not move.

Accuracy of a ray tracing method is directly proportional to the optical path length (OPL) and accuracy of our alignment system is given by

$$\Delta\theta = \frac{\Delta x}{L_1} = \frac{0.3 \text{ mm}}{600 \text{ mm}} = 0.0005 = 0.0005 \text{ rad} \cong 1.7' \quad (2)$$

where Δx is alignment error and L_1 is the OPL (see Figure 4.4). In Figure 4.6, we used 5-hole block to increase the OPL. Incident ray from positive y hole at the 5-hole block reflected by flat mirror and it return back to the negative y hole at the 5-hole block.

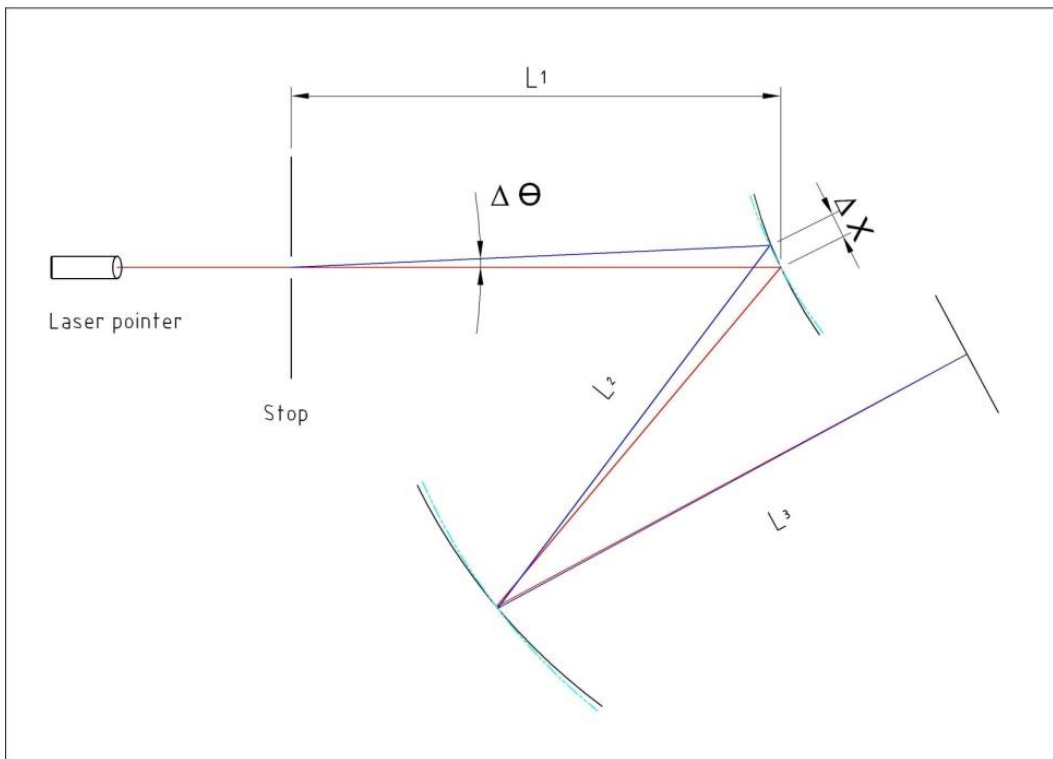
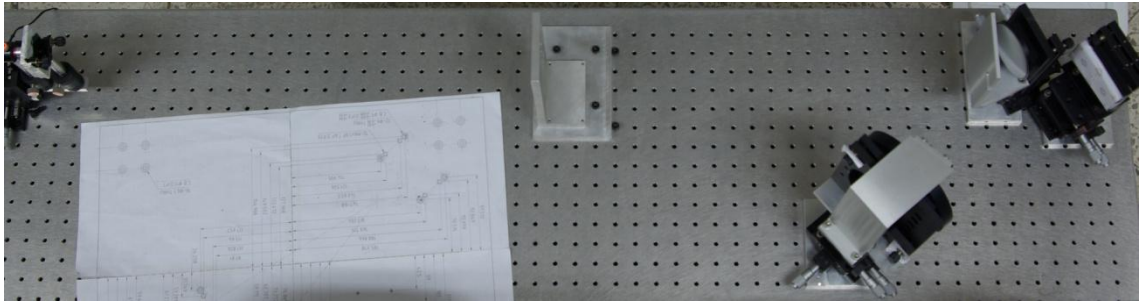
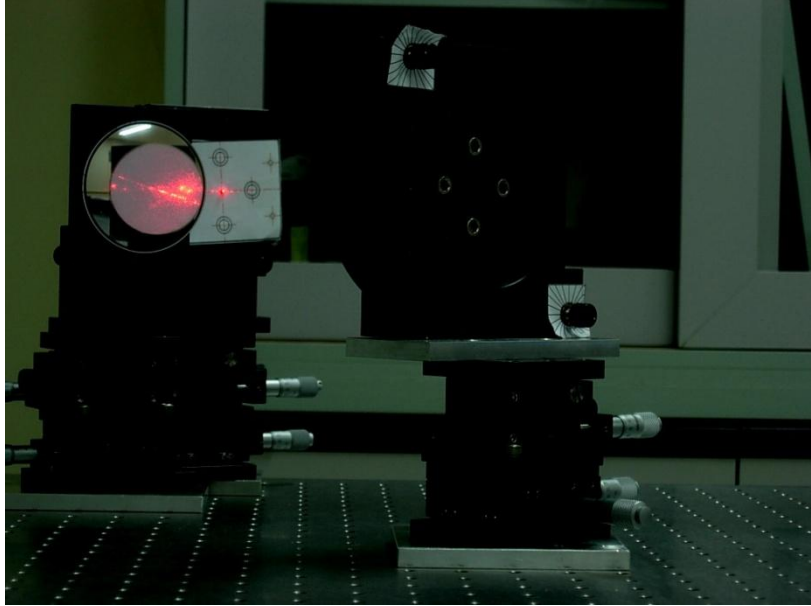


Figure 4.4 Arrangement for a ray tracing method. Top of the image is real image to align the Schwarzschild-Chang type off-axis reflecting telescope. Bottom is illustration of top image and alignment accuracy of a ray tracing method is expressed by Equation 2.

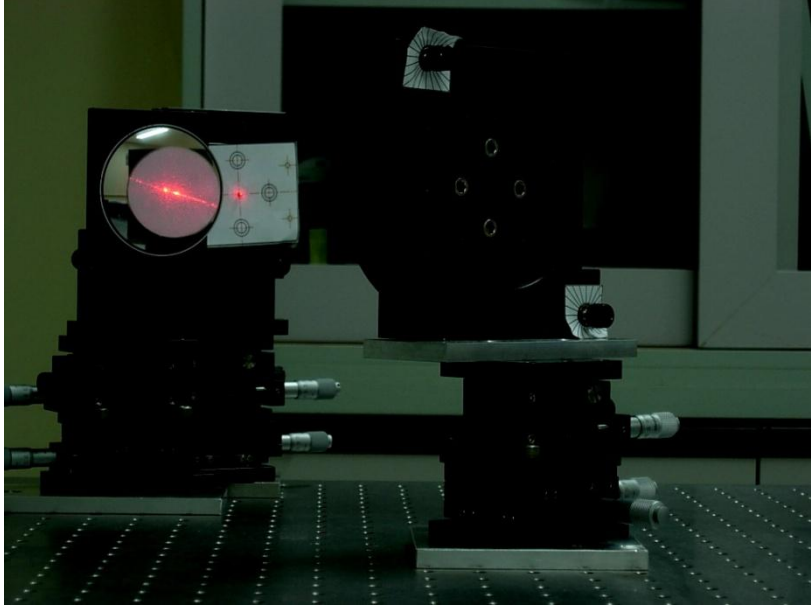


(a)



(b)

Figure 4.5 Ray tracing process: (a) Incident ray from negative y ; (b) Enlarged focus of (a).

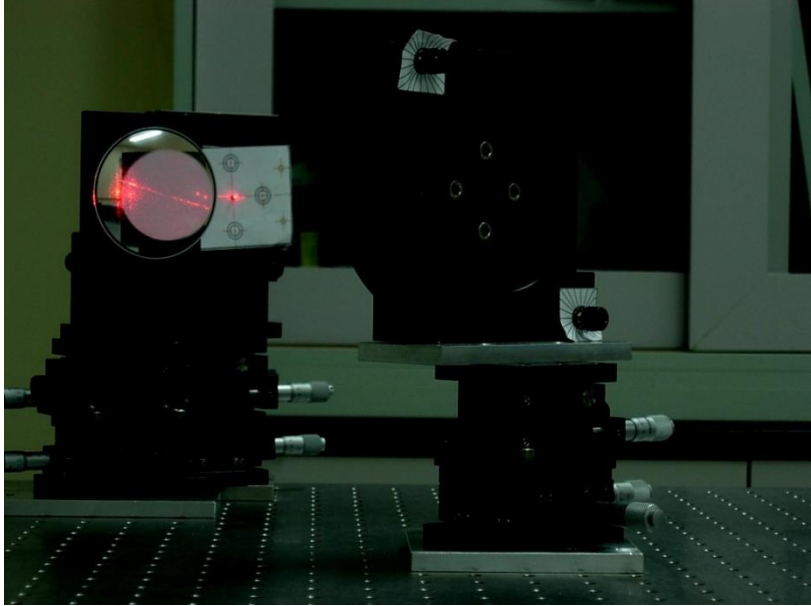


(c)

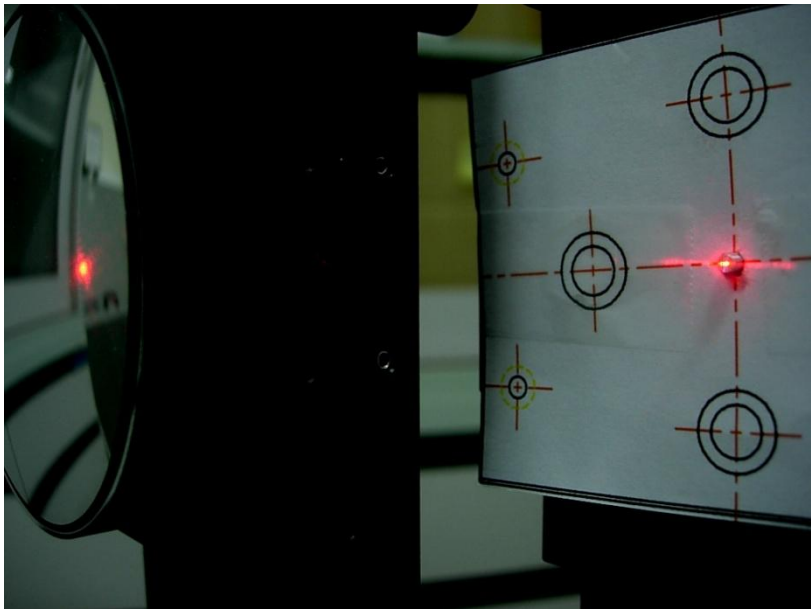


(d)

Figure 4.5 (c) Incident ray from origin; (d) Enlarged focus of (a).



(e)



(f)

Figure 4.5 (e) Incident ray from positive y ; (f) Enlarged focus of (a).

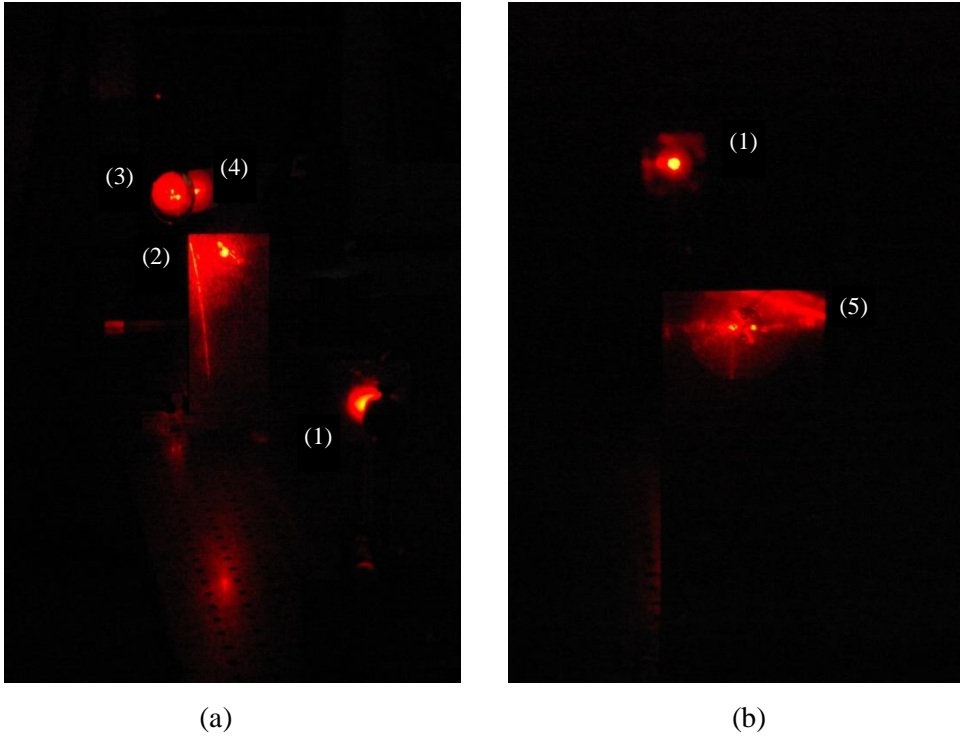
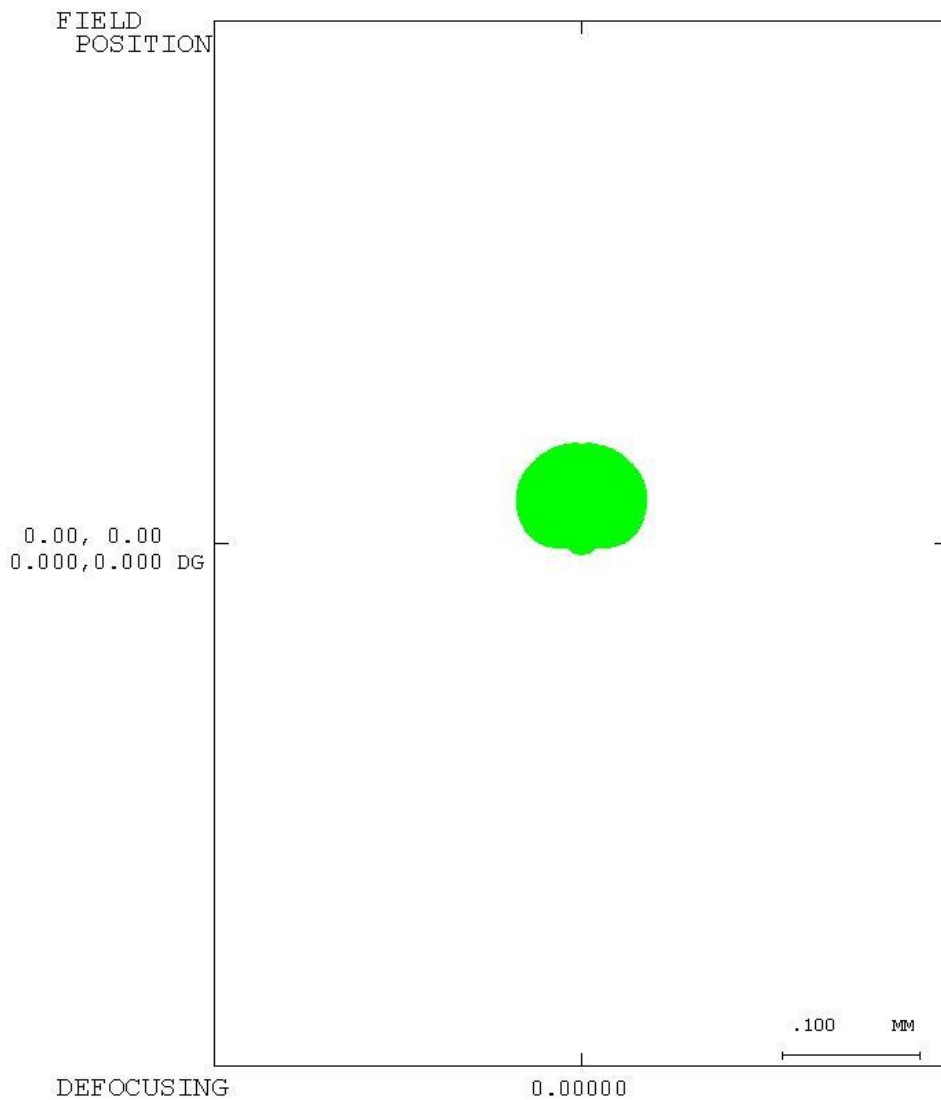


Figure 4.6 Ascertainment of alignment using 5-hole block. (1) is a source, (2) is a stop, (3) is a primary mirror, (4) is a focal plane and (5) is a 5-hole block: (a) The ray from the laser pointer incident to the negative y hole of 5-hole block and return back to the positive y hole of 5-hole block; (b) Close up image of (a) at the back side of stop. We can ascertain negative y and positive y holes are brighter than another holes of the 5-hole block.

5. Point source image test and result

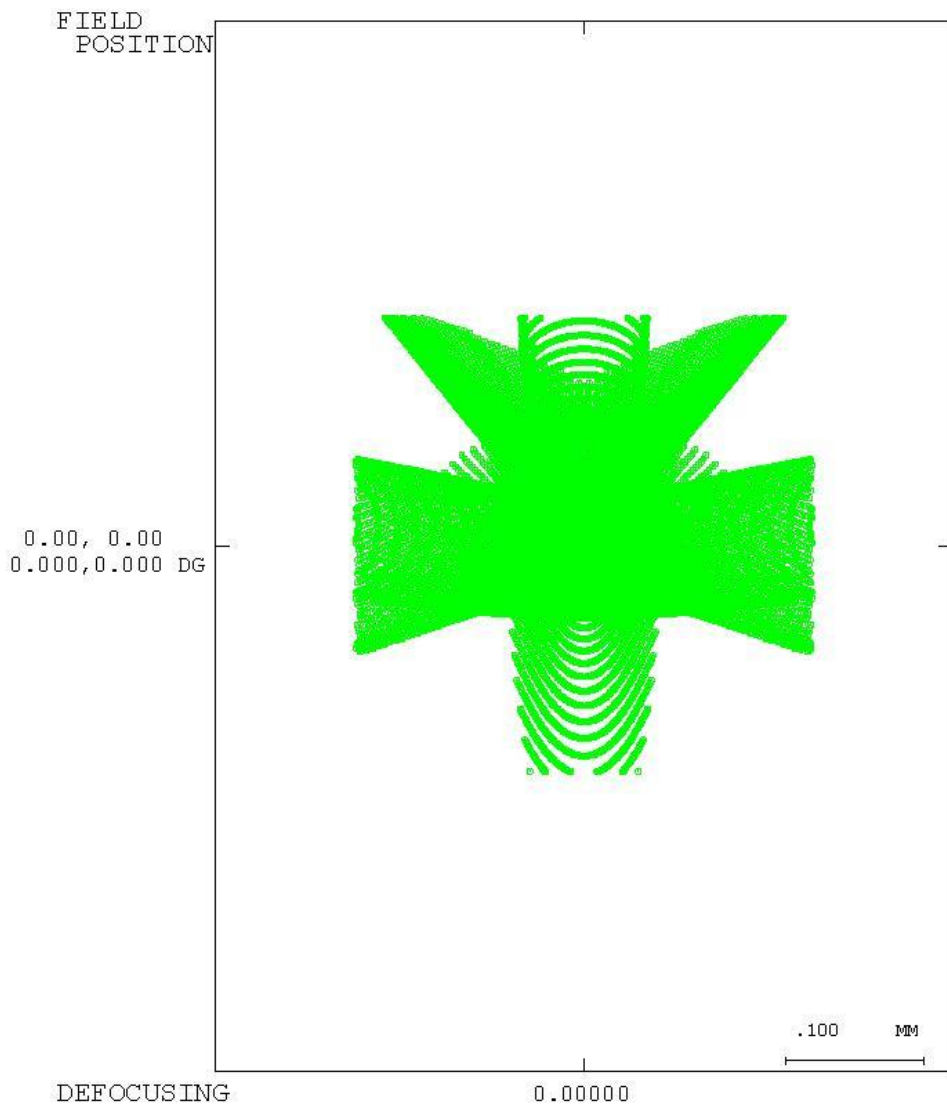
We made point source using laser pointer and optical jumper cord. And optical jumper cord is 1250 mm distant from the primary mirror. Primary and secondary center hole blocks, stop and 5-hole block are removed. And flat mirror replaced with detector. Detector is 2K by 1K charge coupled device (CCD) and pixel size is 3.5 μm . Conditions, like gamma, exposure time, resolution, of detector can set up by the own software. The position of primary and secondary mirrors and stages are not changed. We optimized telescope changing BFL at the object distance 1250 mm in Code V simulation.

When distance of the point source is 1250 mm 84% encircled energy diameter of the Schwarzschild-Chang type off-axis reflecting telescope size of the is 55.5 μm for 632.8 nm wavelength (see Figure 5.1). But 84% encircled energy diameter of the off-axis reflecting telescope which uses derived surface is 110 μm at the same condition in Code V simulation (see Figure 5.2). And spot diameter of off-axis reflecting telescope which uses the fabricated mirrors is 105 μm at the test (see Figure 5.3). The results of the Code V simulation and point source test are arranged at Table 5.1.



Schwarzschild-Chang D50 F2

Figure 5.1 Spot image of the Schwarzschild-Chang type off-axis reflecting telescope. Distance of the point source is 1250 mm from the primary mirror.



Schwarzschild-Chang D50 F2

Figure 5.2 Spot image of the off-axis reflecting telescope which uses derived surface functions in Code V simulation. Distance of the point source is 1250 mm from the primary mirror.

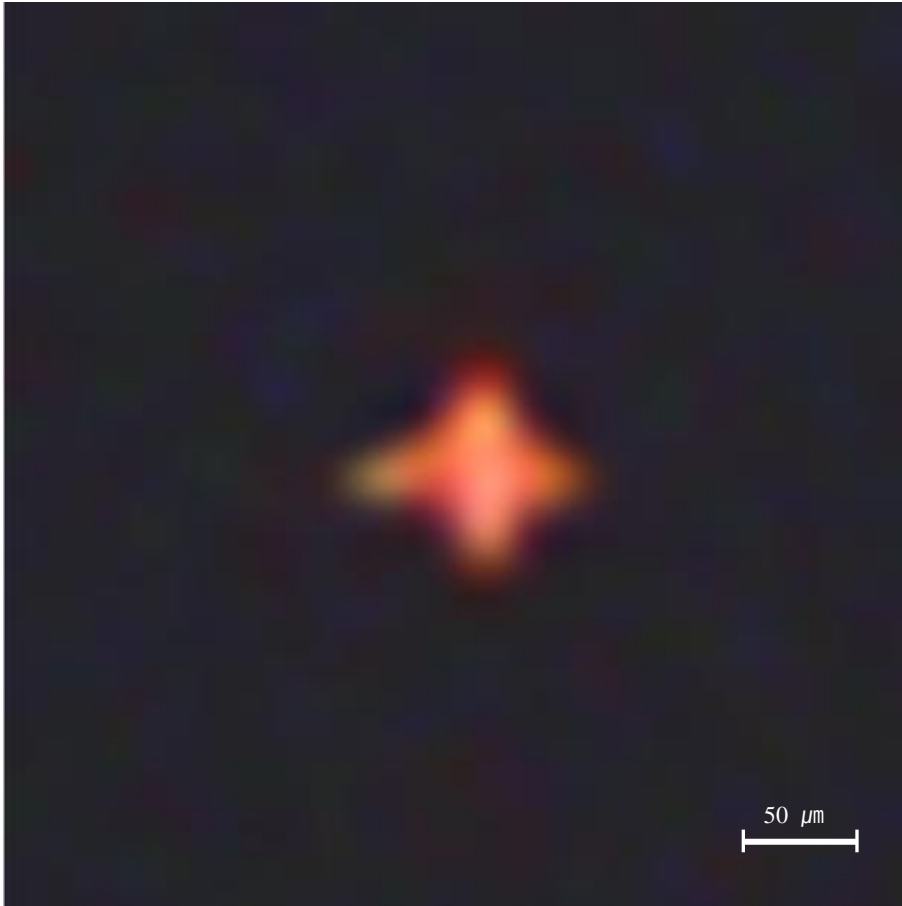


Figure 5.3 Point source test image of the Schwarzschild-Chang type off-axis reflecting telescope which uses fabricated mirrors. Distance of the point source is 1250 mm from the primary mirror and wavelength of point source is 632.8 μm.

Type	Conditions		EED [μm]
	Wavelength	DOS	
The Schwarzschild-Chang type off-axis reflecting telescope	632.8 nm	infinite	3.28 (84%)
The off-axis reflecting telescope using fitted surface functions	632.8 nm	infinite	105 (84%)
The Schwarzschild-Chang type off-axis reflecting telescope	632.8 nm	1250 mm	55.5 (84%)
The off-axis reflecting telescope using derived surface functions	632.8 nm	1250 mm	110 (84%)
The off-axis reflecting telescope using the fabricated mirrors	632.8 nm	1250 mm	105
The Schwarzschild-Chang type off-axis reflecting telescope	10000 μm	infinite	51.5 (84%)
The off-axis reflecting telescope using fitted surface functions	10000 μm	infinite	116 (84%)

Table 5.1 Results of the Code V simulation and point source test. DOS is distance of the source.

6. Conclusion

In this paper, we have developed the off-axis reflecting telescope which has advantages in infrared comparing with refracting or on-axis reflecting telescope. Our telescope is developed for infrared observation and has wide FOV. The optical design of our telescope is the Schwarzschild-Chang type. Off-axis mirrors are manufactured at KBSI. We measured fabricated mirror surfaces and form accuracies of the primary and secondary mirrors are RMS $0.19\ \mu\text{m}$ and RMS $0.72\ \mu\text{m}$. We analyzed for the measured data of the fabricated mirror surfaces to fit the surface functions. The derived surface functions are compared with the designed surfaces functions and the measured data of the fabricated mirror surfaces. Differences of the fitted surface functions and the measured data of the manufactured mirror surfaces are about RMS $0.27\ \mu\text{m}$ for primary and RMS $0.37\ \mu\text{m}$ for secondary. Even though the periphery on the fitted mirror surfaces are off by hundreds of nanometers from the designed shapes, the derived surface areas in the central parts agree well with those of the optical design. The derived surface functions are applied to the surface parameters of the Schwarzschild-Chang type design in the ray-tracing program for optimization and simulation. We have accomplished alignment of the two-mirror off-axis reflecting telescope using a ray tracing method. The accuracy of our alignment system is about 1.7 arcminute and it is satisfied comparing with the result of tolerance analysis. We performed point source test using the fabricated mirrors and compare the point source image with the result of the simulation which uses the derived surface functions. When the distance of the point source is 1250 mm, the spot size of the telescope using the fabricated mirrors is $105\ \mu\text{m}$ for 632.8 nm wavelength and 84 % EED of the telescope which uses the fitted surface functions is $110\ \mu\text{m}$ at the same conditions in simulation. The 84 % EED of the off-axis reflecting telescope using the derived surface functions ($116\ \mu\text{m}$) is approximately two times bigger than the 84 % EED of the Schwarzschild-Chang type off-axis reflecting telescope

(51.5 μm) when the wavelength and the distance of the point source is 10 μm and infinity in simulation. The result of simulation is acceptable because the pixel size of our array is 50 μm .

We had two big problems in development of the Schwarzschild-Chang type off-axis reflecting telescope. The first one was fabrication of the off-axis mirrors. But the off-axis mirrors are fabricated directly using DTM. And the form accuracy and surface roughness of manufactured mirrors are acceptable for IR band. The second one is alignment of system. We performed alignment using ray tracing method. The fitted surface functions which are derived using measured data of fabricated mirrors applied to the Schwarzschild-Chang type off-axis reflecting telescope for simulation and test. We ascertained that alignment was completed and fitted surface functions represent fabricated mirrors well. In view of the results, our off-axis reflecting telescope has no problem in using for IR band.

7. Bibliography

Bass, M., Van Stryland, E. W., Williams, D. R., et al. 1995, "Handbook Of Optics", New York, McGraw-Hill INC.

Clampin, M. 2008, *Advances in Space Research*, Vol. 41, 1983

Chang, S. 2006, *Proc. SPIE*, Vol. 6265, 128

Chang, S. & Prata, A. Jr. 2004, *JOSA A*, Vol.22, 2454

Chang, S., Lee, S. P., Kim, S. P., et al. 2006, *Applied Optics*, Vol.45, 484

Didkovsky, L., Kuhn, J. & Goode, P. 2004, *Proc. SPIE*, Vol. 5171, 333

Fanson, J., Fazio, G., Houck, J., et al. 1998, *Proc. SPIE*, Vol. 3356, 478

Glass, I.S. 1999, "Handbook of Infrared Astronomy", New York, Cambridge University Press

Kim, G. H., Yang, S. C., Kim, H. S., et al. 2007, *JKSPE*, Vol. 24, No. 2, 25

Kim, G. H. 2003, PhD. thesis

Kessler, M.F., Steinz, J.A., Anderegg, M.E., et al. 1996 *A&A*, Vol. 315, No.2, L27

Keil, S. L., Rimmele, T., Keller, C., et al. 2003, *Proc. SPIE*, Vol. 4853, 240

Kuhn, J. R. & Hawley, S. L. 1999, *PASP*, 111, 601

- Kuhn, J. R. & Moretto, G. 2000, Proc. SPIE, Vol. 4003, 324
- Lee, Yeon H. 1992, Optical Engineering, Vol. 31, No. 11, 2287
- Lena, P. 1988, "Observational Astrophysics", Berlin, New York, Springer-Verlag
- Nakagawa, T. & Murakami, M. 2007, AdSpR, Vol. 40, 679
- Neugebauer, G. & Beckin, N. 1971, ARA&A, Vol. 9, 67
- Neugebauer, G., Habing, H. J., Duinen, R. Van, et al. 1984, ApJ, 278, L1
- Moretto, G. & Kuhn, J. R. 1999, Proc. SPIE, Vol. 3785, 75
- Moretto, G. , Langlois, M. & Ferrari, M. 2004, Proc. SPIE, Vol. 5487, 1111
- Murakami, H., Baba, H., Barthel, P., et al. 2007, PASJ Vol. 59, S369
- Schroeder, D. J. 2000, "Astronomical Optic", San Diego, Academic Press
- Tofani, G. & Natale, V. 2003, Memorie della Societa Astronomica Italiana, Vol. 74, 219
- Tsutsumi, H., Yoshizumi, K. & Takeuchi, H. 2005, Proc. SPIE, Vol. 5638, 387
- Yang, S. C., Kim, G. H., Kim, H. S., et al. 2007, JKSP, Vol. 24, No. 2, 19